On the propagation of a coupled saturation and pressure front

D. W. Vasco, Lawrence Berkeley National Laboratory, Berkeley, CA 94720

Abstract. Using an asymptotic technique, valid for a medium with smoothly varying heterogeneity, I derive an expression for the velocity of a propagating, coupled saturation and pressure front. Due to the nonlinearity of the governing equations, the velocity of the propagating front depends upon the magnitude of the saturation and pressure changes across the front in addition to the properties of the medium. Thus, the expression must be evaluated in conjunction with numerical reservoir simulation. The propagation of the two-phase front is governed by the background saturation distribution, the saturation-dependent component of the fluid mobility, the porosity, the permeability, the capillary pressure function, the medium compressibility, and the ratio of the slopes of the relative permeability curves. Numerical simulation of water injection into a porous layer saturated with a non-aqueous phase liquid indicates that two modes of propagation are important. The fastest mode of propagation is a pressure-dominated disturbance that travels through the saturated layer. This is followed, much later, by a coupled mode with a large saturation change. These two modes are also observed in a simulation using a heterogeneous porous layer. A comparison between the propagation times estimated from the results of the numerical simulation and predictions from the asymptotic expression indicates overall agreement.

1. Introduction

In a wide range of activities, including environmental remediation, the geological sequestration of carbon dioxide, and geothermal energy development, it is important to correctly model the flow of fluids within the subsurface. To this end, one must adequately characterize the flow properties at depth. This is typically accomplished through solving an inverse problem in which observations are used to constrain medium parameters, such as the formation permeability [Sun, 1994]. Inverse modeling has advanced in recent years through improved field methods and the development of flexible modeling techniques. For example, there are networks of multi-level samplers and crosswell configurations of transducers capable of generating adense array of observations[Hsieh et al., 1985; Butler et al., 1999; Karasaki et al., 2000; Yeh and Liu, 2000; Vesselinov et al., 2001; Datta-Gupta et al., 2002]. In addition, geophysical measurements have been used to augment hydrological data, to characterize flow properties in the subsurface [Paillet, 1993; Kowalsky et al., 2004; 2005]. Such measurements include satellite-based observations of surface deformation due to seasonal effects, pumping, and fluid injection [Schmidt and Burgmann, 2003; Bell et al., 2008; Vasco et al., 2010; Rucci et al., 2010].

Given the wide variety of geophysical and hydrological data, access to flexible and efficient approaches for modeling and inversion is essential. While purely numerical methods provide the most comprehensive solutions to multiphase flow problems, they tend to be computationally intensive and provide less insight and flexibility. Analytic solutions can be efficient, but are usually limited to fairly simple situations, such as linearized perturbations on a homogeneous background model. There are semi-analytic techniques for modeling and inversion that display some of the efficiency and insight of analytic methods while extending to the more complicated situations that can be treated by numerical techniques. One class of semi-analytic methods, the trajectory-based approaches described in Cohen and Lewis [1967], Shen [1983], Vasco and Datta-Gupta [1999], Vasco et al. [1999], and Vasco et al. [2000], has the additional flexibility of partitioning the inverse problem into a travel time matching problem [Brauchler et al., 2003] and an amplitude matching problem [Vasco, 2008a]. As noted by Cheng et al. [2005], the travel time problem is quasi-linear and thus converges more readily than the highly nonlinear amplitude matching problem. Furthermore, inverting travel times is much more efficient than amplitude inversion and such inverse problems form the basis of medical imaging [Arridge, 1999] and geophysical tomography [Iyer and Hirahara, 1993].

While asymptotic, trajectory-based solutions have been used to treat inverse problems in hydrology [Vasco, 2008b], there are some limitations in current derivations. These limitations are associated with the application of asymptotic techniques to nonlinear problems, such as multiphase flow and coupled processes, (e.g., deformation and flow. Specifically, while asymptotic techniques are applicable to nonlinear processes [Whitham 1974; Anile et al., 1993], and have been applied to two-phase flow [Vasco et al, 1999; Vasco, 2004], the applications have been limited in some respects. For example, capillary effects were neglected in Vasco et al. [1999]. And typically when capillary effects are included, background fields, such as the initial saturation and the capillary pressure, are assumed to be uniform [Anile et al., 1993; Vasco, 2004]. Furthermore, when the governing equation is written in terms of a distinct saturation equation, as in Vasco [2004], the resulting equation for the saturation front velocity is a complicated expression that contains an implicit dependence on the solution of the pressure equation. In this paper I present a new derivation of a trajectory-based solution for two-phase flow in the presence of capillary forces. The derivation is based upon a general approach applicable to any set of coupled nonlinear partial differential equations. The resulting expression for the phase velocity depends explicitly upon the saturation and pressure amplitude changes in a

rather simple fashion. Due to the presence of the saturation and pressure terms, the phase velocity must be calculated in conjunction with the results from a numerical simulator. However, the expression provides insight into the way in which saturation and pressure changes control the propagation of a coupled two-phase front.

2. Methodology

In this section I present the governing equations for two-phase flow and outline an asymptotic analysis based upon the method of multiple scales. The details of the analysis are given in full in Appendix A.

2.1. The Equations Governing Two-Phase Flow

To begin, I consider the set of simultaneous partial differential equations describing the flow of a wetting phase and a non-wetting phase [*Bear*, 1972; *Peaceman*, 1977; *de Marsily*, 1986]

$$\begin{aligned} \nabla \cdot \left[\frac{\rho_w k k_{rw}}{\mu_w} \nabla \left(P_w - \rho_w g z \right) \right] &= \frac{\partial (\rho_w \phi S_w)}{\partial t} \\ \nabla \cdot \left[\frac{\rho_n k k_{rn}}{\mu_n} \nabla \left(P_n - \rho_n g z \right) \right] &= \frac{\partial (\rho_n \phi S_n)}{\partial t} \end{aligned} \tag{1}$$

where S_w and S_n denote the saturation of the wetting and non-wetting phases, respectively. The relative permeabilities of the wetting and non-wetting phases, which are functions of the saturations, are represented by k_{rw} and k_{rn}, while the permeability is given by $k(\mathbf{x})$. The respective densities are ρ_w and ρ_n, the gravitational constant is g and the porosity is $\phi(\mathbf{x})$. The pressure associated with the wetting phase is $P_w(\mathbf{x}, t)$ while the non-wetting phase pressure is $P_n(\mathbf{x}, t)$, the fluid viscosities are μ_w and μ_n. The two equations are coupled because the two fluids are assumed to fill the available pore space and thus, their saturations sum to unity

$$S_w + S_n = 1. \tag{2}$$

I also assume that the phases are incompressible so that their densities are constant. I define the saturation-dependent component of the fluid mobilities [*Peaceman*, 1977, p. 18] by the ratios

$$\eta_w = \frac{k_{rw}}{\mu_w} \tag{3}$$

and

$$\eta_n = \frac{k_{rn}}{\mu_n}. \tag{4}$$

I shall assume that the relative permeability properties are constant for a given formation. Thus, within a given heterogeneous layer I shall assume that the relative permeabilities are only functions of the fluid saturations. Because the saturations sum to unity, I can write the governing equations (1) in terms of one of the saturations, say

$$S = S_w = 1 - S_n \tag{5}$$

and hence the system of equations reduces to two equations in three unknowns

$$\begin{aligned} \nabla \cdot \left[k \eta_w \left(\nabla P_w - \rho_w \mathbf{Z} \right) \right] &= S \frac{\partial \phi}{\partial t} + \phi \frac{\partial S}{\partial t} \\ \nabla \cdot \left[k \eta_n \left(\nabla P_n - \rho_n \mathbf{Z} \right) \right] &= (1 - S) \frac{\partial \phi}{\partial t} - \phi \frac{\partial S}{\partial t} \end{aligned} \tag{6}$$

where $\mathbf{Z} = g \nabla z$ is a vector in the dirction of the gravitational attraction, and I have made use of the definitions (3) and (4) and factored out the fluid densities, as they are constant.

To reduce the system (6) to two equations in two unknowns, I invoke the assumption that the fluid pressure difference, the capillary pressure, P_c, in the pores is a function of the fluid saturation [*Bear*, 1972], thus

$$P_c(S) = P_n - P_w. \tag{7}$$

As was done for the relative permeabilities, I shall assume that the capillary pressure function only varies across a layer boundary and does not depend explicitly upon the spatial location within a particular formation. Rather, in a given formation the capillary pressure function is only a function of the pressure in one fluid phase and the saturation distribution within the layer. Denoting the fluid pressure in the wetting phase by P

$$P = P_w \tag{8}$$

and writing the fluid pressure for the non-wetting phase

$$P_n = P + P_c, \tag{9}$$

I can reduce the system of equations (6) to two equations in two unknowns. First, because of equation (7), I write the gradient of the fluid pressure of the non-wetting phase in terms of the gradients of the pressure and saturation of the wetting phase:

$$\nabla P_n = \nabla P + \frac{\partial P_c}{\partial S} \nabla S. \tag{10}$$

Using equations (8) and (9), and substituting for ∇P_n in the system of equations (6), gives the following equations for S and P

$$\begin{aligned} \nabla \cdot \left[k \eta_w \left(\nabla P - \rho_w \mathbf{Z} \right) \right] &= S \frac{\partial \phi}{\partial t} + \phi \frac{\partial S}{\partial t} \\ \nabla \cdot \left[k \eta_n \left(\nabla P + \gamma_c \nabla S - \rho_n \mathbf{Z} \right) \right] &= (1 - S) \frac{\partial \phi}{\partial t} - \phi \frac{\partial S}{\partial t} \end{aligned} \tag{11}$$

where

$$\gamma_c = \frac{\partial P_c}{\partial S}. \tag{12}$$

As in *de Marsily* [1986], I assume linear elastic behavior for the porous matrix to arrive at a relationship between a change in fluid pressure and a change in matrix porosity. The exact relationship is

$$\frac{\partial \phi}{\partial t} = \alpha_T \frac{\partial P_w}{\partial t}, \tag{13}$$

where α_T is a proportionality coefficient that depends upon the compressibilities of the fluids and the solid, and the porosity. A careful analysis in *de Marsily* [1986, p. 107] indicates that α_T is of the form

$$\alpha_T = \phi \left(\beta_l - \beta_s + \frac{\alpha}{\phi} \right) \tag{14}$$

where β_l is the fluid compressibility, β_s is the compressibility coefficient of the solid grains, and α is the compressibility of

the solid matrix. Substituting (13) for the time derivative of the porosity ϕ, equation (11) becomes

$$\nabla \cdot [k\eta_w (\nabla P - \rho_w \mathbf{Z})] = \alpha_T S \frac{\partial P}{\partial t} + \phi \frac{\partial S}{\partial t}$$

$$\nabla \cdot [k\eta_n (\nabla P + \gamma_c \nabla S - \rho_n \mathbf{Z})] = \alpha_T (1 - S) \frac{\partial P}{\partial t} - \phi \frac{\partial S}{\partial t}. \tag{15}$$

Carrying out the differentiations associated with the outer divergence operator, I can write equation (15) as the following pair of equations

$$\nabla\kappa \cdot \nabla P + \chi_w \nabla S \cdot \nabla P + \nabla \cdot \nabla P - \rho_w \nabla\kappa \cdot \mathbf{Z} - \rho_w \chi_w \nabla S \cdot \mathbf{Z} = \frac{\alpha_T}{k\eta_w} S \frac{\partial P}{\partial t} + \frac{\phi}{k\eta_w} \frac{\partial S}{\partial t} \tag{16}$$

$$\nabla\kappa \cdot \nabla P + \chi_n \nabla S \cdot \nabla P + \nabla \cdot \nabla P - \rho_n \nabla\kappa \cdot \mathbf{Z} - \rho_n \chi_n \nabla S \cdot \mathbf{Z} + \gamma_c \nabla\kappa \cdot \nabla S + \Upsilon \nabla S \cdot \nabla S + \gamma_c \nabla \cdot \nabla S = \frac{\alpha_T}{k\eta_n} (1 - S) \frac{\partial P}{\partial t} - \frac{\phi}{k\eta_n} \frac{\partial S}{\partial t} \tag{17}$$

where

$$\kappa = -\ln k, \tag{18}$$

$$\chi_w = -\frac{\partial \eta_w}{\partial S}, \tag{19}$$

$$\chi_n = -\frac{\partial \eta_n}{\partial S}, \tag{20}$$

and

$$\Upsilon = \gamma_c \chi_n + \frac{\partial \gamma_c}{\partial S}. \tag{21}$$

Equations (16) and (17), comprise the governing equations and serve as the starting point for my application of the method of multiple scales, an asymptotic technique described next.

2.2. An Asymptotic Analysis of the Governing Equations

The governing equations (16) and (17) are rather complicated as they are nonlinear, of mixed character, and coupled partial differential equations with spatially-varying coefficients. Without some manner of simplification an analytic solution is certainly not possible. Because one goal of this work is to develop techniques to solve inverse problems, for example using the saturation front arrival time to infer the flow properties of the medium, retaining the heterogeneity is essential. However, due to the limited resolution of most inverse methods, in which a finite number of data are used to estimate a field of properties, one typically seeks models with smoothly varying heterogeneity. Thus, I am most interested in two-phase flow in a model with smoothly varying properties. I should note that sharp boundaries, in the form of layering, are allowed as explicit boundary conditions.

I can build the assumption of smoothly varying heterogeneity into the modeling through a technique known as the method of multiple scales [*Anile et al.*, 1993]. This approach is suited to the construction of asymptotic solutions for a porous medium with heterogeneous, yet smoothly varying, flow properties. The measure of smoothness is with respect to the scale-length of the two-phase front. In order to define this formally, I first denote the scale-length of the two-phase front, the distance over which the saturation changes from the background value to the value behind the front, by l. In addition, let L denote the scale-length of the heterogeneity within the medium. The smoothness of the medium is stipulated by the requirement that $L >> l$. An asymptotic solution can be formulated in terms of the ratio of scale-lengths $\varepsilon = l/L$. To this end, I will define the slow spatial coordinates

$$\mathbf{X} = \varepsilon \mathbf{x}, \tag{22}$$

the scale over which many of the quantities of interest, such as the travel time and the amplitude will vary. Similarly, I can define a slow time:

$$T = \varepsilon t. \tag{23}$$

An asymptotic solution is a power series representation of the dependent variables, that is, the saturation and pressure. The power series is in terms of the scale variable ε, for example the saturation is represented as

$$S(\mathbf{X}, T, \theta_s) = S_b(\mathbf{X}, T) + \int_0^T e^{\theta_s(\mathbf{X},u)} \sum_{i=0}^{\infty} \varepsilon^i S_i(\mathbf{X}, u) du \tag{24}$$

where S_b is the background saturation that may be a function of space and time, $\theta_s(\mathbf{X}, T)$ is a phase function that is related to the propagation time of the saturation front, and $S_i(\mathbf{X}, T)$ is the i-th contribution to the saturation amplitude. The integral appears in the representation because I will be considering a step-function source, rather than a pulse-like source. The saturation contains both an explicit and an implicit dependence upon the spatial and temporal coordinates. The implicit dependence is through the phase function $\theta_s(\mathbf{X}, T)$. The representation (24) is in the form of a traveling front, a propagating change in the saturation with respect to the background saturation.

The increase in pressure across the two-phase front has a similar representation

$$P(\mathbf{X}, T, \theta_p) = P_b(\mathbf{X}, T) + \int_0^T e^{\theta_p(\mathbf{X},u)} \sum_{i=0}^{\infty} \varepsilon^i P_i(\mathbf{X}, u) du. \tag{25}$$

Note that the phase function for the pressure can differ from the saturation phase, meaning that the saturation and pressure can move with different speeds. This allows the jump in pressure to propagate much faster then the saturation change for example. Later in the paper I will examine the situation in which $\theta_s = \theta_p$.

The governing equations can be re-written in terms of the slow coordinates. In order to do this I first express the partial derivatives in terms of X_i, T, and θ. In doing so I make use of the relationships (22) and (23) between the fast and slow coordinates and the explicit and implicit dependence upon the independent variables. Thus, I can write the partial derivative with respect to time as

$$\frac{\partial S}{\partial t} = \varepsilon \frac{\partial S}{\partial T} + \frac{\partial \theta_s}{\partial t} \frac{\partial S}{\partial \theta_s} \tag{26}$$

because, from the definition of T, equation (23), $\partial T/\partial t = \varepsilon$. Similarly, I can express the derivative with respect to x_i as

$$\frac{\partial S}{\partial x_i} = \varepsilon \frac{\partial S}{\partial X_i} + \frac{\partial \theta_s}{\partial x_i} \frac{\partial S}{\partial \theta_s}, \tag{27}$$

and thus the gradient in terms of the $\mathbf{X}$ coordinates is given by

$$\nabla_X S = \varepsilon \nabla_x S + \nabla\theta_s \frac{\partial S}{\partial \theta_s}. \tag{28}$$

Given these expressions for the differential operators I can rewrite the governing equations in terms of the slow variables $\mathbf{X}$ and T. Each term will contain a factor that is the scale parameter ε raised to some power. Because we are assuming that the saturation and pressure fronts vary over a scale length that is much less then that of the heterogeneity, ε is assumed to be much smaller than one. Therefore, terms of low order in ε will dominate in the governing equations. In Appendix A, I write the governing equations in terms of the slow variables and retain terms of lowest order in ε. In order to derive an expression for the travel time of the capillary front, the following will be limited to terms of order ε^0. To order ε^0 the governing equations take the form [see Appendix A for a complete treatment]

$$\chi_w \mathbf{s}\cdot\mathbf{p}\bar{S}\bar{P} + p^2\bar{P} - \rho_w\chi_w \mathbf{s}\cdot\mathbf{Z}\bar{S} = \frac{\alpha_T}{k\eta_w} S\bar{P}\frac{\partial\theta_p}{\partial t} + \frac{\phi}{k\eta_w}\bar{S}\frac{\partial\theta_s}{\partial t} \tag{29}$$

$$\chi_n \mathbf{s}\cdot\mathbf{p}\bar{S}\bar{P} + p^2\bar{P} + \rho_n\chi_n \mathbf{s}\cdot\mathbf{Z}\bar{S} + \Upsilon s^2\bar{S}^2 + \gamma_c s^2\bar{S} = \frac{\alpha_T}{k\eta_n}(1-S)\bar{P}\frac{\partial\theta_p}{\partial t} - \frac{\phi}{k\eta_n}\bar{S}\frac{\partial\theta_s}{\partial t} \tag{30}$$

where I have defined the gradient vectors of the phase functions θ_p and θ_s

$$\mathbf{p} = \nabla\theta_p \tag{31}$$

and

$$\mathbf{s} = \nabla\theta_s \tag{32}$$

with magnitudes $s = |\mathbf{s}|$ and $p = |\mathbf{p}|$, respectively. The quantities $\bar{S}$ and $\bar{P}$, defined by

$$\bar{S} = S_0 - S_b \tag{33}$$

and

$$\bar{P} = P_0 - P_b, \tag{34}$$

signify the change in saturation and pressure from the background values to new values due to the passage of the two-phase front.

2.3. An Expression Governing the Evolution of the Two-Phase Front

The two equations (29) and (30) provide relationships between the gradients of the phase functions, $\mathbf{s}$ and $\mathbf{p}$ and the amplitudes of the saturation and pressure changes, $\bar{S}$ and $\bar{P}$, across the front. In this sub-section I use equations (29) and (30) to derive explicit expressions for the magnitude of the slowness vectors, s and/or p in terms of the medium and fluid properties and the amplitude changes $\bar{S}$ and $\bar{P}$. The quantity s is the front slowness, the inverse of the front velocity, an important quantity for calculating the travel time of the two-phase front.

However, before delving into a detailed derivation, I need to discuss an important issue regarding the nature of the propagating front. As noted above, it is assumed that the leading edge of the front is defined by a rapid jump in saturation and pressure. Ahead of the front, the saturation and pressure are at their background values, behind the front the saturation and/or pressure assume new values, different from the background values. The concept of a propagating front has proven extremely useful in a wide variety of fields, such as electromagnetics [*Kline and Kay*, 1965; *Luneburg*, 1966], and is central to many treatments of nonlinear wave propagation [*Whitham*, 1974; *Maslov and Omel'yanov*, 2001]. Many of the coefficients, for example χ_w, γ_c, and Υ, in equations (29) and (30) are functions of the saturation and pressure. Thus, there is the question of what values of saturation and pressure should be used in determining the coefficients? Because I am interested in the arrival time of the leading edge of the front, which evolves according to the saturation and pressure encountered before the jump to new values, I will use the background conditions to compute the coefficients in (29) and (30).

Fixing the coefficients in equations (29) and (30) to their background values, the next task involves estimating the slowness of the propagating front. If the governing equations were linear differential equations, then the zeroth order terms would form a linear system and one could use the condition that the linear system have a non-trivial solution to find the admissible slowness values [*Kline and Kay*, 1965; *Kravtsov and Orlov*, 1990]. A formal approach, similar to that used for linear systems of equations, may be based on techniques from algebraic geometry [*Cox et al.*, 1998]. Equations (29) and (30) comprise two quadratic equations in $\bar{S}$ and $\bar{P}$. The condition that the two polynomial equations (29) and (30) have common zeros, and thus solutions, is the vanishing of the resultant [*Cox et al.*, 1998; *Sturmfels*, 2002]. The resultant is the determinant of a matrix whose entries are the coefficients in equations (29) and (30) and powers of one of the variables, either $\bar{S}$ and $\bar{P}$. Thus, the resultant is a polynomial equation in s, p with coefficients that depend upon either $\bar{S}$ or $\bar{P}$ and the properties of the medium. The condition of the vanishing of the resultant generalizes the vanishing of a determinant of the coefficient matrix of a linear system of equations [*Noble and Daniel*, 1977].

Here I take a direct approach, first solving equation (29) for the product term

$$\mathbf{s}\cdot\mathbf{p}\bar{S}\bar{P} = \frac{1}{\chi_w}\left[\frac{\alpha_T}{k\eta_w}S_b\bar{P} + \frac{\phi}{k\eta_w}\bar{S} - p^2\bar{P} - \rho_w\chi_w\mathbf{s}\cdot\mathbf{Z}\bar{S}\right], \tag{35}$$

where I have used the background value S_b for the saturation. Substituting this expression for $\mathbf{s}\cdot\mathbf{p}\bar{S}\bar{P}$ into equation (30) and grouping terms according to their degrees in s and p gives

$$\left(\Upsilon\bar{S} + \gamma_c\right)\bar{S}s^2 + \left(1 - \frac{\chi_n}{\chi_w}\right)\bar{P}p^2 + \chi_n\mathbf{s}\cdot\mathbf{Z}\left(\rho_n - \rho_w\right)\bar{S}s - \frac{\alpha_T}{k}\left(\frac{1-S_b}{\eta_n} - \frac{\chi_n}{\chi_w}\frac{S_b}{\eta_w}\right)\bar{P}\frac{\partial\theta_p}{\partial t} + \frac{\phi}{k}\left(\frac{\chi_n}{\chi_w}\frac{1}{\eta_w} + \frac{1}{\eta_n}\right)\bar{S}\frac{\partial\theta_s}{\partial t} = 0, \tag{36}$$

an equation for the slownesses.

In the most general situation, in which no assumptions are made regarding $\mathbf{s}$ and $\mathbf{p}$, there more unknowns then there are equations. However, I am primarily interested in the propagation of a two-phase front in which the change in saturation and the change in pressure are coupled. That is, the jump in saturation and pressure occur simultaneously as the front passes. Thus, θ_s and θ_p, the phase terms associated with the saturation and pressure changes, are equal $\theta_s = \theta_p = \theta$, $\nabla\theta_s = \mathbf{s} = \mathbf{p} = \nabla\theta_p$ and $s = p$. In that case equation (36) reduces to a single equation that is quadratic in p

$$\left[\left(1 - \frac{\chi_n}{\chi_w}\right)\bar{P} + \left(\Upsilon\bar{S} + \gamma_c\right)\bar{S}\right]p^2 + \chi_n\mathbf{p}\cdot\mathbf{Z}\left(\rho_n - \rho_w\right)\bar{S}p$$

$$-\frac{\alpha_T}{k}\left(\frac{1-S_b}{\eta_n}-\frac{\chi_n}{\chi_w}\frac{S_b}{\eta_w}\right)\bar{P}\frac{\partial\theta_p}{\partial t}+\frac{\phi}{k}\left(\frac{\chi_n}{\chi_w}\frac{1}{\eta_w}+\frac{1}{\eta_n}\right)\bar{S}\frac{\partial\theta_s}{\partial t}=0. \tag{37}$$

Defining the ratio

$$\chi=\frac{\chi_n}{\chi_w} \tag{38}$$

and the coefficients

$$\Gamma=\frac{\chi_n\left(\rho_n-\rho_w\right)\bar{S}}{\left(1-\chi\right)\bar{P}+\left(\Upsilon\bar{S}+\gamma_c\right)\bar{S}} \tag{39}$$

and

$$\Omega=\frac{\alpha_T\left[\left(1-S_b\right)\eta_n{}^{-1}-\chi S_b\eta_w{}^{-1}\right]\bar{P}-\phi\left[\chi\eta_w{}^{-1}+\eta_n{}^{-1}\right]\bar{S}}{k\left[\left(1-\chi\right)\bar{P}+\left(\Upsilon\bar{S}+\gamma_c\right)\bar{S}\right]}, \tag{40}$$

I can write equation (37) as

$$p^2+\Gamma g\cos(\zeta)p-\Omega\frac{\partial\theta}{\partial t}=0, \tag{41}$$

where I have used the fact that $\mathbf{p}\cdot\mathbf{Z}=g\cos\zeta$. The quantity ζ signifies the angle between the slowness vector $\mathbf{p}$ and the direction of the gravitational attraction $\mathbf{Z}$. As shown in the next sub-section, this expression can be used, in conjunction with a numerical reservoir simulator, to compute the slowness, and hence the velocity of the propagating two-phase front. In particular, one can use a numerical simulator to calculate the saturation and pressure changes over the region of interest due to the passage of the two-phase front. Thus, one obtains estimates of $\bar{S}$ and $\bar{P}$ which may be substituted into the expressions (39) and (40). Equation (41) for the slowness is fairly general, allowing for both capillary effects as well as gravitational forces.

2.4. The Computation of the Phase Function

Recalling the definition of the phase gradient vector $\mathbf{p}$, given by (31), one observes that equation (41) is a differential equation for the phase function $\theta(\mathbf{X},t)$

$$\nabla\theta\cdot\nabla\theta+\Gamma\nabla\theta\cdot\mathbf{Z}-\Omega\frac{\partial\theta}{\partial t}=0. \tag{42}$$

Equation (42) is an example of a Hamilton-Jacobi differential equation, a class of equations that are of fundamental importance in many areas of physics [*Lanczos*, 1986]. Hamilton-Jacobi equations have a well-developed mathematical foundation [*Courant and Hilbert*, 1962; *Sneddon*, 2006, p. 81] that underlies ray methods in electromagnetic [*Kline and Kay*, 1965; *Luneburg*, 1966] and elastic [*Karal and Keller*, 1959; *Kravtsov and Orlov*, 1990] wave propagation.

The most direct method for solving equation (42) is a numerical approach, based upon finite-differences. Such methods, which have grown in popularity since their inception [*Crandall and Lions*, 1983; *Crandall et al.*, 1984; *Vidale*, 1988; *Sethian*, 1990; *van Trier and Symes*, 1991], are now well developed [*Sethian*, 1999]. Techniques, such as the fast marching method and level set methods [*Sethian*, 1999] are general and applicable to equations such as (42). I should note that techniques developed for static Hamilton-Jacobi equations, equations that do not depend upon time, can be applied to equation (42) by treating the temporal variable t simply as an additional spatial variable [*Sethian*, 1999, p. 99]. The fact that the gravitational term results in preferential movement in the direction of $\mathbf{Z}$ presents no fundamental difficulty. There are a number of implementations of finite-difference-based algorithms for anisotropic propagation, commonly used in seismic wave propagation in an anisotropic Earth [*Lecomte*, 1993; *Eaton*, 1993; *Qian and Symes*, 2001; *Soukina et al.*, 2003]. Preferential propagation in a horizontal or vertical direction is also a factor in anisotropic crystal growth and finite-difference schemes have been used to model such propagation [*Sethian and Strain*, 1992].

The classical alternative to a finite-difference approach is to solve equation (42) using the method of characteristics [*Courant and Hilbert*, 1962, p. 63]. As shown here, such an approach leads to a trajectory-based solution and an alternative numerical technique for solving the Hamilton-Jacobi equation (42). In the case of (42), the dependent variable θ does not appear explicitly and I can applied the simplified approach described in *Courant and Hilbert* [1962, p. 106]. I first write equation (42) in the form

$$\frac{\partial\theta}{\partial t}-H(\mathbf{x},t,\mathbf{p})=0 \tag{43}$$

where $H(\mathbf{x},t,\mathbf{p})$ is the Hamiltonian function, given by

$$H(\mathbf{x},t,\mathbf{p})=\Omega^{-1}\mathbf{p}\cdot\mathbf{p}+\Psi\mathbf{p}\cdot\mathbf{Z} \tag{44}$$

and

$$\Psi(\mathbf{x},t)=\Omega^{-1}(\mathbf{x},t)\Gamma(\mathbf{x},t). \tag{45}$$

The characteristic equations corresponding to the scalar partial differential equation (43), are a set of ordinary differential equations

$$\frac{dx_i}{dt}=-\frac{\partial H}{\partial p_i} \tag{46}$$

$$\frac{dp_i}{dt}=\frac{\partial H}{\partial x_i} \tag{47}$$

that follow from geometrical arguments. Making use of the particular form of the Hamiltonian, equation (44), I can write equations (46) and (47) in vector form as

$$\frac{d\mathbf{x}}{dt}=-2\Omega^{-1}\mathbf{p}-\Psi\mathbf{Z} \tag{48}$$

$$\frac{d\mathbf{p}}{dt}=p^2\nabla\Omega^{-1}+\mathbf{p}\cdot\mathbf{Z}\nabla\Psi. \tag{49}$$

These two sets of differential equations define the system of rays, that is the trajectories over which the solutions are defined. The vector function $\mathbf{x}(t)$ defines a curve through the model which describes the propagation of the coupled front. The system of ordinary equations may be solved numerically, using techniques for two-point boundary value problems [*Press et al.*, 1992,p. 745]. Note that the two sets of equations (48) and (49) display preferential flow in the $\mathbf{Z}$ direction due to gravitational forces. This preferential flow introduces an anisotropy and modifies the trajectories. The situation is similar to that of wave propagation in an anisotropic medium and has been treated in studies of wave propagation in an anisotropic Earth [*Cerveny*, 1972; *Chapman and Pratt*, 1992].

Once the trajectories between a source and an observation point have been computed, and the slowness vector defined, the method of characteristics can be used to compute the phase. The defining equations are the two scalar ordinary differential equations

$$\frac{d\theta}{dt}=-\sum_{i=1}^{3}p_i\frac{\partial H}{\partial p_i}+H \tag{50}$$

and

$$\frac{dp_t}{dt} = \frac{\partial H}{\partial t} \tag{51}$$

[*Courant and Hilbert*, 1962, p. 106]. For the particular Hamiltonian given above, one arrives at

$$\frac{d\theta}{dt} = p^2 \Omega^{-1} \tag{52}$$

and

$$\frac{dp_t}{dt} = p^2 \frac{\partial \Omega^{-1}}{\partial t}. \tag{53}$$

Integrating (52) produces an expression for θ in terms of the medium properties, as contained in the function Ω

$$\theta(\mathbf{x}(t), t) = \int_0^t \frac{p^2}{\Omega} du. \tag{54}$$

Note that, if gravity is not important, for example if the densities are close in value, or if the flow is restricted to a narrow horizontal layer, equations (48) and (49) still apply, however Ψ will vanish. Therefore, the flow will be controlled by Ω and there will be no preferential flow in the $\mathbf{Z}$ direction. In that case it is possible, under certain circumstances, to write the phase function in a separable form, such as $\theta(\mathbf{x}, t) = \beta(t)\sigma^2(\mathbf{x})$. In Appendix B I derive an explicit expression for $\theta(\mathbf{x}, t)$ for the case in which the phase is a separable function. In Appendix B, it is shown that

$$\beta(t) = -\frac{1}{t}$$

and

$$\sigma(\mathbf{x}) = \int_{\mathbf{x}} \sqrt{\Omega} ds,$$

resulting in

$$\theta(\mathbf{x}(s), t) = -\frac{1}{4t} \left(\int_{\mathbf{x}(s)} \sqrt{\Omega} ds \right)^2, \tag{55}$$

is similar to the phase function for the linear diffusion equation [*Vasco et al.*, 2000].

2.5. A Zeroth-Order Solution for the Saturation and Pressure Changes

Armed with expressions for the trajectory of the propagating front and the phase function $\theta(\mathbf{x}, t)$, one can construct a low order representation of the saturation and pressure fields using the series solutions (24) and (25). Because I am interested in solutions for a model with smoothly varying flow properties, ε is assumed to be small, and thus the first few terms of the series dominate. Here I consider a zeroth-order solution, only taking the first term of each series. The expression for the saturation change with respect to the background value $S_b(\mathbf{X}, T)$, is

$$\bar{S}(\mathbf{X}, T, \theta_s) = \int_0^T e^{\theta_s(\mathbf{X}, u)} S_0(\mathbf{X}, u) du, \tag{56}$$

and similarly for the pressure change

$$\bar{P}(\mathbf{X}, T, \theta_p) = \int_0^T e^{\theta_p(\mathbf{X}, u)} P_0(\mathbf{X}, u) du. \tag{57}$$

Note that these solutions are incomplete because they depend upon the amplitudes S_0 and P_0 which are not provided. In fact, the defining equation for the phase, equation (42) contains coefficients Γ and Ω that depend upon the amplitude changes $\bar{S}$ and $\bar{P}$. Thus, the expression (56) and (57) must be evaluated in conjunction with estimates of the amplitude changes S_0 and P_0. For example, in the next section I will use the numerical simulator TOUGH2 [*Pruess et al.*, 1999] to calculate the amplitude changes.

One can gain some physical insight into the meaning of the phase terms θ_s and θ_p following a line of reasoning first suggested by *Virieux et al.* [1994]. Before discussing their approach in detail, I note that each of the semi-analytic expressions (56) and (57) are integrals with respect to time of an exponential of the phase function multiplied by an amplitude function. The exponential of the phase function is always a positive number and the amplitude function is typically of one sign for a passing front. For example, the amplitude function S_0 will either describe a decrease or an increase in the saturation of the aqueous phase, depending on the nature of the passing coupled front. The point is that the integrals are typically piece-wise monotonic if the coupled multiphase front is due to the injection of a particular fluid component.

As noted in *Vasco et al.* [2000] and *Vasco and Finsterle* [2004], the transient, wave-like nature of a solution to the diffusion equation is emphasized by taking the derivative of the head or pressure with respect to time. Thus, I shall be interested in the time-derivative of the saturation and pressure changes, which are of the form

$$\frac{\partial \bar{S}(\mathbf{X}, T, \theta_s)}{\partial t} = e^{\theta_s(\mathbf{X}, T)} S_0(\mathbf{X}, T) \tag{58}$$

and

$$\frac{\partial \bar{P}(\mathbf{X}, T, \theta_p)}{\partial t} = e^{\theta_p(\mathbf{X}, T)} P_0(\mathbf{X}, T). \tag{59}$$

For a separable phase function, as given by equation (55), the saturation and pressure resemble the product of a Gaussian function and the time-varying amplitude function.

If the amplitude functions $S_0(\mathbf{X}, T)$ and $P_0(\mathbf{X}, T)$ vary monotonically as functions of time, then the derivatives (58) and (59) should display single peaks, associated with the peak of each Gaussian function. I can derive equations for the peaks by differentiating the expressions (58) and (59) and setting the result to zero. For example, differentiating (58) with respect to time

$$\frac{\partial^2 \bar{S}}{\partial t^2} = e^{\theta_s} \left[S_0 \frac{\partial \theta_s}{\partial t} + \frac{\partial S_0}{\partial t} \right]. \tag{60}$$

The exponential term in (60) is non-zero as long as one stays away from the origin. Thus, the condition for the peak of the time derivative of $\bar{S}$ is

$$\frac{\partial^2 \bar{S}}{\partial t^2} = S_0 \frac{\partial \theta_s}{\partial t} + \frac{\partial S_0}{\partial t} = 0. \tag{61}$$

In order to derive a specific expression relating the phase to the peak of the time derivative of the saturation, I shall need to introduce additional assumptions. In the next subsection I consider one possible form for the amplitude function $S_0(\mathbf{X}, t)$, a power-law time-dependence. Other amplitude functions, such as a form based upon Hermite polynomials, are possible.

2.5.1. A Power-Law Time-Dependence

Motivated by the solution to the linear diffusion equation [*Vasco et al.*, 2000], I consider the specific form

$$S_0(\mathbf{X}, t) = t^{-\alpha_s} S_x(\mathbf{X}) \tag{62}$$

where α_s is constant and $S_x(\mathbf{X})$ is a function of $\mathbf{X}$. Thus, for an amplitude function of the form (62), equation (61) becomes

$$\frac{\partial^2 \bar{S}}{\partial t^2} = t^{-\alpha_s} \frac{\partial \theta_s}{\partial t} + \alpha_s t^{-\alpha_s - 1} = 0. \tag{63}$$

Third, I assume that the phase function $\theta_s(\mathbf{X}, t)$ can be written in the separable form, $\theta(\mathbf{x}, t) = \beta(t)\sigma^2(\mathbf{x})$, as derived in Appendix B. With these three assumptions, equation (61) reduces to

$$\frac{\partial^2 \bar{S}}{\partial t^2} = \frac{\sigma^2}{4} - \alpha_s t = 0. \tag{64}$$

I can relate the phase component $\sigma(\mathbf{X})$ to the time at which the time-derivative of the saturation is a maximum or minimum. I denote the time at which the derivative is a peak as T_{peak}. The specific relationship is

$$\sigma = 2\sqrt{\alpha_s T_{peak}}, \tag{65}$$

or, solving for T_{peak} and using the definition of σ, given by (B16),

$$\sqrt{T_{peak}} = \frac{1}{2\sqrt{\alpha_s}} \int_{\mathbf{x}(s)} \sqrt{\Omega} ds. \tag{66}$$

Thus, under the stated assumptions, the time derivative of the saturation is a maximum at the time T_{peak} and this time is determined by the medium parameters, as contained in Ω, by equation (66). A similar analysis can be applied to the pressure variation, under the corresponding assumption that the pressure amplitude has the separable form

$$P_0(\mathbf{X}, t) = t^{-\alpha_p} P_x(\mathbf{X}) \tag{67}$$

where $P_x(\mathbf{X})$ is the spatial component of the pressure amplitude function. The resulting peak time for the pressure time derivative is

$$\sqrt{T_{peak}} = \frac{1}{2\sqrt{\alpha_p}} \int_{\mathbf{x}(s)} \sqrt{\Omega} ds, \tag{68}$$

which is similar to the expression for the linear diffusion equation [*Vasco et al.*, 2000].

3. Applications

In this section I illustrate how one can use the expression for the slowness, equation (41), to calculate the travel time of a coupled pressure and saturation disturbance. For simplicity, I shall neglect gravitational effects, so that equation (41) reduces to

$$p^2 - \Omega \frac{\partial \theta}{\partial t} = 0. \tag{69}$$

In the examples that follow I shall consider the injection of water into a layer containing a non-aqueous phase liquid (NAPL). The numerical simulator TOUGH2 [*Pruess et al.*, 1999] is used to model the flow of the two-phases in response to the injection. The relative permeability functions $k_{rw}(S)$ and $k_{rn}(S)$ are plotted in Figure 1. The relative permeability of the non-aqueous phase liquid is given by the default formulation of TOUGH2 [*Pruess et al.*, 1999, p. 50] for oil,

$$k_{rn}(S) = \frac{1 - S - S_{nr}}{1 - S_{nr}} \tag{70}$$

where S_{nr} is the residual saturation of the NAPL. The relative permeability function of *Corey* [1954] is used to model the water,

$$k_{rw}(S) = \hat{S}^4, \tag{71}$$

where

$$\hat{S} = \frac{S - S_{wr}}{1 - S_{wr} - S_{gr}} \tag{72}$$

and $S_{wr} = 0.2$ and $S_{gr} = 0.1$.

A central well, indicated by a star in Figure 2, injects water at a rate of 4.0 kg/s. The injection starts at time zero and continues at a constant rate. Thus, the source behaves as a step-function in time. Two observation points, located to the north of the injector, are denoted by the open and filled circles in Figure 2. Due to the injection, saturation and pressure changes propagate from the injection well into the porous layer. The water saturation and pressure distributions, after 100 days of injection, are shown in Figure 2.

The saturation changes and the pressure calculated at the first observation point, denoted by the filled circle in Figure 2, are shown in Figure 3. Note that saturation and pressure changes occur soon after the start of injection. Initially, there is a small decrease in water saturation at the observation point. However, a large, rapid saturation increase occurs around 250 days after the start of injection. In contrast, the pressure builds up gradually and monotonically over time. Careful examination of the pressure variation in Figure 3, indicates a change in the rate of pressure build-up at around 250 days. As noted above, and in previous publications [*Vasco et al.*, 2000; *Vasco and Finsterle*, 2004; *Vasco*, 2008a], the propagation of transient pressure changes are clearer if one considers the time derivative of the pressure history. To this end, I plot the time derivative of both the saturation and pressure changes in Figure 4. Note that the time derivative of the pressure displays two peaks, the first at an early time (less than 100 days), and the second around 300 days. The derivative of the saturation change, shown in Figure 4a, displays similar characteristics, in this case a trough at an early time and a peak at around 300 days. In the next sub-section I shall examine the early changes, that I refer to as the first arrival, in more detail. Because the change in saturation associated with the early disturbance is quite small, less than 5 %, the flow in this case is dominated by the larger change in pressure.

3.1. Flow Dominated by a Change in Pressure

The changes at early times are associated with the transient pressure disturbance propagating in the non-aqueous phase liquid, well ahead of the injected water front. That is, the saturation and pressure changes are dominated by pressure propagation in the background saturation distribution. There is also a small saturation change driven by the pressure changes, inducing relative flow of the two phases. In this sub-section I shall consider these changes and interpret them in terms of the expressions for the travel time and phase velocity.

The early peak in the pressure derivative in Figure 4 is shown in greater detail in Figure 5. In Figure 5 I have also plotted the early decrease in saturation seen in Figure 4a. Both of these curves have been normalized to unit amplitude and converted so that they are positive. Note how closely the pressure change follows the saturation change in time (Figure 5), with a peak value at around 50 days. One can also consider snapshots of the normalized saturation and pressure derivatives in the layer. Specifically, I plot the normalized saturation and pressure derivatives in each grid block at particular times, as done in Figures 6

and 7. These snapshots convey the transient propagation of the saturation and pressure changes. That is, the peak of the saturation and pressure derivatives propagates outward from the injection well over time. Furthermore, the changes in saturation and pressure are coupled and move with the same velocity. That is to be expected because the saturation changes are induced by the propagating pressure changes. Noting the time as which the normalized derivative of the saturation and pressure in each grid block attains a maximum value, I can compute the arrival time of the disturbances at each point in the layer (Figure 8). The arrival times are very similar for the early-time saturation and pressure changes.

Using the expressions for Ω, equation (40), and the travel times [equations (66) and (68)], one can estimate the arrival times for the saturation and pressure changes. When there is only a small saturation change associated with the propagating front, I can approximate the coefficient Ω by

$$\Omega = \frac{\alpha_T \left[(1 - S_b)\, {\eta_n}^{-1} - \chi S_b {\eta_w}^{-1} \right]}{k\,(1 - \chi)}, \tag{73}$$

where α_T is the coefficient given by equation (14):

$$\alpha_T = \phi \left(\beta_l - \beta_s + \frac{\alpha}{\phi} \right). \tag{74}$$

Note that expression (73) only depends upon the properties of the medium. As noted by *Vasco and Finsterle* [2004] one can use the arrival time field estimated from the output of the numerical simulator to compute the trajectories $\mathbf{x}(t)$ mentioned above. In Figure 8 I have plotted the trajectory from the second observation point, denoted by the open circle, to the injection well, denoted by the star. Because the layer is homogeneous the trajectory is a straight line. Using the expressions (73) and (68) I can estimate the travel time, assuming that the pressure disturbance travels in the same manner as a solution to the diffusion equation

$$\sqrt{T_p} = \frac{1}{6} \int_{\mathbf{x}} \sqrt{\frac{\alpha_T \left[(1 - S_b)\, {\eta_n}^{-1} - \chi S_b {\eta_w}^{-1} \right]}{k\,(1 - \chi)}} ds. \tag{75}$$

In Figure 9 I compare travel times estimated using equation (75) to estimates extracted from the output of the TOUGH2 numerical simulation. The values are computed for the points along the trajectory shown in Figure 8. In general, there is good agreement between the semi-analytic estimates, based upon equation (75), and the estimates from the numerical simulator.

3.2. Fully Coupled Saturation and Pressure Changes

Now consider the second arrival in Figure 4, associated with the propagating saturation front. One can no longer assume that the saturation change is small. Neither can one assume that the pressure change in negligible due to its large magnitude. To some degree I can isolate the pressure change by calculating the pressure field in the layer due to the injection of fluid of the same composition. Thus, I can estimate the component of the pressure change due to the fluid mass change with no corresponding saturation change. In Figure 10 I compare the derivative of this differential pressure, normalized such that the peak of the time derivative is unity, to the normalized time derivative of the saturation change. The removal of the pressure change due to the fluid mass change is imperfect, however, in general there is good agreement between saturation and pressure. As for the earlier phase, I can examine snapshots of the saturation and pressure time derivatives as they vary over the simulation grid (Figure 11 and 12). Again, the propagation of the disturbance is apparent in the snapshots, as is the agreement between the saturation and pressure changes. Note that the propagation away from the injection point is not entirely symmetric, indicating some anisotropy, likely due to numerical grid effects. This effect could possibly be minimized by taking a finer simulation grid. In order to minimize the grid effects I consider observation points along the north-south axis of the grid, denoted by the filled and open circles in Figures 11, 12, and 13.

As was done for the earlier arrival, one can post-process the results of the numerical simulation in order to estimate travel times for the propagating disturbances. The simplest approach, and the one taken here, is to take the time at which the time-derivative attains a maximum value as the 'arrival time' of the disturbance. In Figures 13a and 13b I have plotted the travel times associated with the saturation and pressure disturbances, respectively. There is excellent agreement between the two distributions of travel times within the layer. Note that the anisotropy, possible due to numerical grid effects, is reflected in the asymmetry of the travel time contours. The trajectories, computed by marching down gradient of the travel time functions, are also shown in Figure 13. The trajectories denote the path traveled by the saturation and pressure disturbances from the injection well to the outer observation point, denoted by the open circle.

Using the expression for Ω, given by equation (40), one can calculate the travel time from the medium parameters and the changes in saturation and pressure due to the passage of the two-phase front. The model for water and NAPL in TOUGH2 assumes no capillary effects so that the functions γ_c and Υ vanish and Ω takes the form

$$\Omega = \frac{\alpha_T \left[(1 - S_b)\, {\eta_n}^{-1} - \chi S_b {\eta_w}^{-1} \right]}{k\,(1 - \chi)} + \frac{\phi \left[\chi {\eta_w}^{-1} + {\eta_n}^{-1} \right] \bar{S}}{k\,(1 - \chi)\, \bar{P}}. \tag{76}$$

From (76) and the relationship between Ω and T_{peak}, as given in equation (68), it is clear that the second term is responsible for the additional time taken to travel from the injection well to the observation point. The amplitude changes $\bar{S}$ and $\bar{P}$ were estimated from the numerical simulator output. Specifically, I compute the difference between the field values associated with the arrival time of the front (the time at which the time derivative is a maximum) and the field values before the arrival of the front. In Figure 14 I compare the travel time estimates based upon (76) with the times obtained by post-processing the TOUGH2 numerical simulator saturation and pressure histories. In general, there is rather good agreement and, as is apparent in the saturation and pressure derivatives (Figure 4), the second arrival takes much longer to reach the observation point.

3.3. Flow in a Heterogeneous Medium

As noted above, one motivation for developing semi-analytic solutions is the solution of the inverse problem. That is, one would like to use the explicit expressions to develop efficient and flexible methods for characterization. For this reason, I have allowed for heterogeneity of arbitrary magnitude in the formulation. In this sub-section I consider a heterogeneous medium, described by a variation in absolute permeability $k(\mathbf{x})$, all other parameters are kept at the values used in the homogeneous case. The smoothly varying model contains generally higher permeability to the west and lower permeability to the east (Figure 15). The lowest permeability is found in the northeast corner of the model. The saturation and pressure variations, in response to water injection in the central well, are influenced by the heterogeneity. This is clear in Figure 16, which displays the

saturation and pressure variations in the layer after 525 days of injection. The fields reflect the heterogeneity, with rapid migration of the two-phase front in the higher permeability region west of the injection well.

The saturation and pressure histories are calculated at an observation point to the north of the injector, indicated by the filled circle in Figure 16. In Figure 17 the time derivatives of the saturation and pressure variations are plotted as a function of time from the start of injection. The overall character of the curves: the two peaks in the pressure derivative and the early decrease in saturation followed by a large and rapid increase, are similar to those found in the homogeneous case (Figure 4). As in the homogeneous case, I can compute the travel times associated with the two sets of extremum in the saturation and pressure variations. For example, the first arrival time is associated with the first peak in the pressure derivative, as seen in Figure 17b, and the early trough in the saturation variation (Figure 17a). The distribution of travel times for the saturation and pressure variations are shown in Figures 18a and 18b, respectively. The distribution of travel times are very similar as are the trajectories computed by marching down the gradient of the travel time field, from an observation point to the injection point (Figure 18). Using equation (75), now with a spatially varying absolution permeability $k(\mathbf{x})$, I can calculate the travel time for the heterogeneous medium. In Figure 19 I compare the estimated travel times to values obtained from the numerical simulation. The travel times are computed for points along the trajectory shown in Figure 18. The asymptotic estimates are in general agreement with travel times obtained from the TOUGH2 simulator output. In general the front moves faster at near and intermediate distances and then slows considerably at farther offsets. This behavior makes physical sense because, as seen in Figure 15, the trajectory encounters lower permeability material as it traverses the northeast quadrant of the simulation grid near the end of the path.

Now I consider the later arrival, exemplified by the second peak in the saturation and pressure derivatives in Figure 17. As noted previously, this disturbance is due to the propagating saturation front and the travel time is related to the variable Ω, given by expression (76). In this case, the absolute permeability, $k(\mathbf{x})$ is a spatially varying quantity. I should point out that the permeability appears both explicitly in the expression (76) as well as implicitly, as the permeability also determines the saturation and pressure amplitude changes, $\bar{S}$, and $\bar{P}$, respectively. Thus, the travel time distribution and the trajectories for this disturbance can differ from those of the first arrival. In fact, the travel time contours and the trajectory for the second arrival (Figure 20) do differ from those of the first arrival (Figure 18). Some of the differences may also be due to grid orientation effects, noted in Figures 11, 12, and 13. In both cases the trajectories curve towards the higher permeability region, away from areas of lower permeability. Using expression (76) I calculate the expected travel time to points along the trajectory, as shown in Figure 21. As in the homogeneous case, the travel time is much greater for the second arrival, due to the presence of the second term in equation (76). Also, as for the first arrival, the disturbance travels faster to near and intermediate points of the trajectory and takes much longer to reach the more distant points.

4. Conclusions

Under the assumption of smoothly varying heterogeneity, it is possible to derive an explicit expression for the phase velocity of a coupled change in saturation and fluid pressure. The expression displays the explicit dependence of the front velocity upon the parameters of the medium and the saturation and pressure changes that occur as the front passes. Due to the presence of the saturation and pressure amplitude changes, the expression for the front velocity is evaluated in conjunction with a numerical simulation. In addition, the presence of the saturation and pressure amplitude means that at least two modes of propagation are possible, depending on the relative magnitude of the saturation and pressure changes. That is, the coupled front can propagate with a different velocity, depending on the size of the saturation change, relative to the change in pressure as the front passes. Numerical simulation using TOUGH2 [*Pruess et al*, 1999], indicates that two modes of propagation are important: the propagation of a pressure-dominated change and the propagation of a coupled front in which the saturation change is large. These conclusions hold for a heterogeneous medium, though the geometry is controlled by the spatial variation of properties. The factors influencing the propagation velocity of the two-phase front are the background saturation, the saturation-dependent components of the fluid mobilities, the medium compressibility, the permeability, the porosity, and the ratio of the slopes of the relative permeability curves at the background saturation.

The technique presented in this paper is general and may be applied to any system of nonlinear partial differential equations. Thus, one may consider coupled processes involving deformation and thermal effects. However, as additional variable and equations are added, the resulting expressions for the phase velocity becomes increasingly complicated. The increased complexity is no different from that seen in linear systems, such as in coupled deformation in a poroelastic medium saturated with two fluid phases [*Tuncay and Corapcioglu*, 1996].

5. Appendix A: The Method of Multiple Scales

5.1. The First of the Governing Equations

Consider the first of the governing equations (16) and it's representation in terms of the slow coordinates $\mathbf{X}$ and T. Substituting for the differential operators in this equation gives the expression

$$\begin{aligned}
&\varepsilon\nabla\kappa\cdot\left(\varepsilon\nabla P+\nabla\theta_p\frac{\partial P}{\partial\theta_p}\right)\\
&+\chi_w\left(\varepsilon\nabla S+\nabla\theta_s\frac{\partial S}{\partial\theta_s}\right)\cdot\left(\varepsilon\nabla P+\nabla\theta_p\frac{\partial P}{\partial\theta_p}\right)\\
&+\varepsilon\nabla\cdot\left(\varepsilon\nabla P+\nabla\theta_p\frac{\partial P}{\partial\theta_p}\right)\\
&+\nabla\theta_p\frac{\partial}{\partial\theta_p}\left(\varepsilon\nabla P+\nabla\theta_p\frac{\partial P}{\partial\theta_p}\right)\\
&-\rho_w\varepsilon\nabla\kappa\cdot\mathbf{Z} \qquad (A1)\\
&-\rho_w\chi_w\left(\varepsilon\nabla S+\nabla\theta_s\frac{\partial S}{\partial\theta_s}\right)\cdot\mathbf{Z}\\
&=\frac{\alpha_T}{k\eta_w}S\left(\varepsilon\frac{\partial P}{\partial T}+\frac{\partial\theta_p}{\partial t}\frac{\partial P}{\partial\theta_p}\right)\\
&+\frac{\phi}{k\eta_w}\left(\varepsilon\frac{\partial S}{\partial T}+\frac{\partial\theta_s}{\partial t}\frac{\partial S}{\partial\theta_s}\right).
\end{aligned}$$

Expanding the product terms and retaining terms of order $\varepsilon^0\sim 1$ gives

$$\chi_w\nabla\theta_s\cdot\nabla\theta_p\frac{\partial S}{\partial\theta_s}\frac{\partial P}{\partial\theta_p}+\nabla\theta_p\cdot\nabla\theta_p\frac{\partial^2 P}{\partial{\theta_p}^2}-\rho_w\chi_w\nabla\theta_s\cdot\mathbf{Z}\frac{\partial S}{\partial\theta_s}$$

$$=\frac{\alpha_T}{k\eta_w}S\frac{\partial\theta_p}{\partial t}\frac{\partial P}{\partial\theta_p}+\frac{\phi}{k\eta_w}\frac{\partial\theta_s}{\partial t}\frac{\partial S}{\partial\theta_s}. \qquad (A2)$$

In what follows I shall need to define the gradient vectors

$$\mathbf{p}=\nabla\theta_p \qquad (A3)$$

and

$$\mathbf{s}=\nabla\theta_s. \qquad (A4)$$

From the particular form of the saturation and pressure, given by the expansions (24) and (25), I note that to order ε^0,

$$\frac{\partial S}{\partial\theta_s}=S_0-S_b=\bar{S} \qquad (A5)$$

and

$$\frac{\partial P}{\partial\theta_p}=P_0-P_b=\bar{P}. \qquad (A6)$$

The quantities $\bar{S}$ and $\bar{P}$ signify the change in saturation and pressure from the background value to the value after the passage of the two-phase front. Incorporating all of these considerations into the expression (A2) produces the more compact expression

$$\chi_w\mathbf{s}\cdot\mathbf{p}\bar{S}\bar{P}+p^2\bar{P}-\rho_w\chi_w\mathbf{s}\cdot\mathbf{Z}\bar{S}=\frac{\alpha_T}{k\eta_w}S\bar{P}\frac{\partial\theta_p}{\partial t}+\frac{\phi}{k\eta_w}\bar{S}\frac{\partial\theta_s}{\partial t} \qquad (A7)$$

where p and s are the magnitudes of the pressure and saturation phase gradient vectors, respectively.

5.2. The Second of the Governing Equations

Now consider the second of the governing equations (17), expressing the differential operators in terms of the slow variables,

$$\begin{aligned}
&\varepsilon\nabla\kappa\cdot\left(\varepsilon\nabla P+\nabla\theta_p\frac{\partial P}{\partial\theta_p}\right)\\
&+\chi_n\left(\varepsilon\nabla S+\nabla\theta_s\frac{\partial S}{\partial\theta_s}\right)\cdot\left(\varepsilon\nabla P+\nabla\theta_p\frac{\partial P}{\partial\theta_p}\right)\\
&+\varepsilon\nabla\cdot\left(\varepsilon\nabla P+\nabla\theta_p\frac{\partial P}{\partial\theta_p}\right)\\
&+\nabla\theta_p\cdot\frac{\partial}{\partial\theta_p}\left(\varepsilon\nabla P+\nabla\theta_p\frac{\partial P}{\partial\theta_p}\right)\\
&-\rho_n\varepsilon\nabla\kappa\cdot\mathbf{Z} \qquad (A8)\\
&-\rho_n\chi_n\left(\varepsilon\nabla S+\nabla\theta_s\frac{\partial S}{\partial\theta_s}\right)\cdot\mathbf{Z}\\
&+\varepsilon\gamma_c\nabla\kappa\cdot\left(\varepsilon\nabla S+\nabla\theta_s\frac{\partial S}{\partial\theta_s}\right)\\
&+\Upsilon\left(\varepsilon\nabla S+\nabla\theta_s\frac{\partial S}{\partial\theta_s}\right)\cdot\left(\varepsilon\nabla S+\nabla\theta_s\frac{\partial S}{\partial\theta_s}\right)\\
&+\varepsilon\gamma_c\nabla\cdot\left(\varepsilon\nabla S+\nabla\theta_s\frac{\partial S}{\partial\theta_s}\right)\\
&+\gamma_c\nabla\theta_s\cdot\frac{\partial}{\partial\theta_s}\left(\varepsilon\nabla S+\nabla\theta_s\frac{\partial S}{\partial\theta_s}\right)\\
&=\frac{\alpha_T}{k\eta_n}(1-S)\left(\varepsilon\frac{\partial P}{\partial T}+\frac{\partial\theta_p}{\partial t}\frac{\partial P}{\partial\theta_p}\right)\\
&-\frac{\phi}{k\eta_n}\left(\varepsilon\frac{\partial S}{\partial T}+\frac{\partial\theta_s}{\partial t}\frac{\partial S}{\partial\theta_s}\right).
\end{aligned}$$

To zeroth-order in ε I obtain the following form for the second governing equation

$$\chi_n\nabla\theta_s\cdot\nabla\theta_p\frac{\partial S}{\partial\theta_s}\frac{\partial P}{\partial\theta_p}+\nabla\theta_p\cdot\nabla\theta_p\frac{\partial^2 P}{\partial{\theta_p}^2}-\rho_n\chi_n\nabla\theta_s\cdot\mathbf{Z}\frac{\partial S}{\partial\theta_s}$$

$$+\Upsilon\nabla\theta_s\cdot\nabla\theta_s\left(\frac{\partial S}{\partial\theta_s}\right)^2+\gamma_c\nabla\theta_s\cdot\nabla\theta_s\frac{\partial^2 S}{\partial{\theta_s}^2} \qquad (A9)$$

$$=\frac{\alpha_T}{k\eta_n}(1-S)\frac{\partial\theta_p}{\partial t}\frac{\partial P}{\partial\theta_p}-\frac{\phi}{k\eta_n}\frac{\partial\theta_s}{\partial t}\frac{\partial S}{\partial\theta_s}.$$

Making the substitutions discussed above [equations (A3) through (A6)], equation (A10) takes the form

$$\chi_n\mathbf{s}\cdot\mathbf{p}\bar{S}\bar{P}+p^2\bar{P}-\rho_n\chi_n\mathbf{s}\cdot\mathbf{Z}\bar{S}+\Upsilon s^2\bar{S}^2+\gamma_c s^2\bar{S}$$

$$=\frac{\alpha_T}{k\eta_n}(1-S)\bar{P}\frac{\partial\theta_p}{\partial t}-\frac{\phi}{k\eta_n}\bar{S}\frac{\partial\theta_s}{\partial t} \qquad (A10)$$

Equations (A7) and (A10) form the starting point for the analysis in the main portion of this paper.

6. Appendix B: Computation of the Phase for a Separable Function

In this Appendix I derive an explicit expression for the phase function $\theta(\mathbf{x}, t)$. In doing so I shall assume a separable form for the phase function

$$\theta(\mathbf{x}, t) = \beta(t)\sigma^2(\mathbf{x}) \tag{B1}$$

and use the separation of variables to solve equation (42). Unfortunately, the gravitational term in equation (42) prevents one from separating the spatial and temporal variables. Therefore, I shall have to neglect gravitational effects, assuming that either the density contrast between the fluid phases is small or that the flow is dominantly horizontal, perpendicular to the gravitational field. In that case, equation (42) reduces to

$$\nabla\theta \cdot \nabla\theta - \Omega\frac{\partial\theta}{\partial t} = 0. \tag{B2}$$

This equation, without gravity, is of sufficient interest and covers a number of important situations that it is worthy of consideration. Furthermore, I treat such problems in the Applications section, where I compare the asymptotic estimates of propagation time with estimates from a numerical simulator. Substituting the separable form (B1) into equation (B2) and noting that

$$\nabla\theta = 2\beta\sigma\nabla\sigma \tag{B3}$$

and

$$\frac{\partial\theta}{\partial t} = \sigma^2\frac{d\beta}{dt}, \tag{B4}$$

where I have used the total derivative for $\beta(t)$ because it only depends upon the single variable t, results in the expression

$$4\beta^2\sigma^2\nabla\sigma \cdot \nabla\sigma - \Omega\sigma^2\frac{d\beta}{dt} = 0, \tag{B5}$$

or

$$\frac{\nabla\sigma \cdot \nabla\sigma}{\Omega} - \frac{1}{4\beta^2}\frac{d\beta}{dt} = 0. \tag{B5}$$

Equation (B5) is separable if Ω is either separable or only depends upon $\mathbf{x}$. The time dependence of Ω enters through the amplitude changes $\bar{P}$ and $\bar{S}$ which multiply each factor. The amplitude changes may not be be functions of time. For example, the change in saturation due to the passage of the front is primarily determined by the pre-existing saturation and by the properties of the relative permeability curves describing the material. Thus, the saturation change $\bar{S}$ is essentially a function of position and does not change significantly as a function of time. That is, the saturation change will be the same, no matter when the two-phase passes through a particular region. Alternatively, during the initiation of injection, a transient pressure change can propagate away from the injection well, accompanied by a very small change in saturation. Thus, the saturation change that occurs due to the passage of the front, $\bar{S}$, is negligible and only the terms associated with $\bar{P}$ are significant. Then the terms $\bar{P}$ will factor out of Ω and the time-dependent terms will cancel.

For situations in which Ω only depends upon $\mathbf{x}$, equation (B5), written as

$$\frac{\nabla\sigma \cdot \nabla\sigma}{\Omega} = \frac{1}{4\beta^2}\frac{d\beta}{dt} \tag{B6}$$

expresses the equality of the left-hand-side, which only depends upon spatial coordinates, $\mathbf{x}$, and the right-hand-side which only depends upon time, t. This means that the terms on either side must equal a constant value, which I denote by C. Thus, for the right-hand-side of equation (B6),

$$\frac{1}{4\beta^2}\frac{d\beta}{dt} = C \tag{B7}$$

or

$$\beta = -\frac{1}{4Ct}. \tag{B8}$$

Similarly, the left-hand-side of equation (B6) produces the partial differential equation

$$\nabla\sigma \cdot \nabla\sigma = C\Omega \tag{B9}$$

known as the eikonal equation [*Kravtsov and Orlov*, 1990]. A solution of the eikonal equation follows from an application of the method of characteristics [*Courant and Hilbert*, 1962, p. 97]. The characteristic equations associated with equation (B9) follow if I define the Hamiltonian function $F(\mathbf{x}, \mathbf{p})$ as

$$F(\mathbf{x}, \mathbf{p}) = \mathbf{p} \cdot \mathbf{p} - C\Omega \tag{B10}$$

with equation (B9) given by $F(\mathbf{x}, \mathbf{p}) = 0$. As noted in *Courant and Hilbert* [1962, p. 97], the characteristic equations are a pair of ordinary differential equations

$$\frac{dx_i}{ds} = \frac{\partial F}{\partial p_i} \tag{B11}$$

$$\frac{dp_i}{ds} = -\frac{\partial F}{\partial x_i} \tag{B12}$$

or, making use of the Hamiltonian function (B10),

$$\frac{d\mathbf{x}}{ds} = 2\mathbf{p} \tag{B13}$$

$$\frac{d\mathbf{p}}{ds} = C\nabla\Omega. \tag{B14}$$

Equation (B13) defines a trajectory, $\mathbf{x}(s)$, over which a solution is constructed. The variable s is the distance along the trajectory. Using the trajectory to define a coordinate system, I can rewrite the eikonal equation (B9), noting that $\mathbf{p}$ is tangent to the trajectory $\mathbf{x}(s)$

$$\frac{d\sigma}{ds} = \sqrt{C\Omega}. \tag{B15}$$

Integrating along the trajectory, I arrive at an expression for $\sigma(\mathbf{x})$

$$\sigma(\mathbf{x}(s)) = \sqrt{C}\int_{\mathbf{x}(s)}\sqrt{\Omega}ds. \tag{B16}$$

Combining the functions (B8) for $\beta(t)$ and (B16) for $\sigma(\mathbf{x})$, produces an expression for the phase $\theta(\mathbf{x}, t)$, [see equation (B1)],

$$\theta(\mathbf{x}(s), t) = -\frac{1}{4t}\left(\int_{\mathbf{x}(s)}\sqrt{\Omega}ds\right)^2. \tag{B17}$$

Acknowledgments. This work was supported by the Assistant Secretary, Office of Basic Energy Sciences of the U. S. Department of Energy under contract DE-AC02-05CH11231.

References

Anile, A. M., J. K. Hunter, P. Pantano, and G. Russo, *Ray Methods for Nonlinear Waves in Fluids and Plasmas*, Longman Scientific and Technical, New York, 1993.

Arridge, S., Optical tomography in medical imaging, *Inverse Problems*, **15**, R41-R93, 1999.

Bear, J., *Dynamics of Fluids in Porous Media*, Dover Publications, 1972.

Bell, J. W., F. Amelung, A. Ferretti, M. Bianchi, and F. Novali, Permanent scatterer InSAR reveals seasonal and long-term aquifer-system response to groundwater pumping and artificial recharge, *Water Resources Research*, **44**, W02407, doi:10.1029/2007WR006152, 2008.

Brauchler, R., R. Liedl, and P. Dietrich, A travel time based hydraulic tomographic approach, *Water Resour. Res., 39*, 1-12, 2003.

Butler, J. J., C. D., McElwee, and G. C. Bohling, Pumping tests in networks of multilevel sampling wells: Motivation and methodology, *Water Resources Research*, **35**, 3553-3560, 1999.

Cerveny, V., Seismic rays and ray intensities in inhomogeneous anisotropic media, *Geophysical Journal of the Royal Astronomical Society*, **29**, 1-13, 1972.

Chapman, C. H., and R. G. Pratt, Traveltime tomography in anisotropic media - I. Theory, *Geophysical Journal International*, **109**, 1-19, 1992.

Cheng, H., Z., He, and A. Datta-Gupta, A comparison of travel-time and amplitude matching for field-scale production data integration: Sensitivity, non-linearity, and practical implications, *Soc. Petrol. Eng. Journal*, **10**, 75-90, 2005.

Cohen, J. K., and R. M. Lewis, A ray method for the asymptotic solution of the diffusion equation, *J. Inst. Math. Applics.*, **3**, 266-290, 1967.

Cory, A. T., The interrelation between gas and oil relative permeabilities, *Producers Monthly*, , 38-41, 1954.

Courant, R., and D. Hilbert, *Methods of Mathematical Physics*, Interscience, New York, 1962.

Cox, D., J. Little, and D. O'Shea, *Using Algebraic Geometry*, Springer, New York, 1998.

Crandall, M. G., and P.-L. Lions, Viscosity solutions of Hamilton-Jacobi equations, *Transactions of the American Mathematical Society*, **277**, 1-43, 1983.

Crandall, M. G., L. C. Evans, and P.-L. Lions, Some properties of viscosity solutions of Hamilton-Jacobi equations, *Transactions of the American Mathematical Society*, **282**, 487-502, 1984.

Datta-Gupta, A., S. Yoon, D. W. Vasco, and G. A. Pope, Inverse modeling of partitioning interwell tracer tests: A streamline approach, *Water Resources Research*, **38**, 1-15, doi:10.1029/2001WR000597,2002.

de Marsily, G., *Quantitative Hydrogeology*, Academic Press, San Diego, 1986.

Eaton, D. W. S., Finite difference travel-time calculation for anisotropic media, *Geophysical Journal International*, **114**, 273-280, 1993.

Hsieh, P. A., S. P. Neuman, G. K. Stiles, and E. S. Simpson, Field determination of the three-dimensional hydraulic conductivity tensor of anisotropic media: 2. Methodology and application to fractured rocks, *Water Resources Research*, **21**, 1667-1676, 1985.

Iyer, H. M., and K. Hirahara, *Seismic Tomography: Theory and Practice*, Chapman & Hall, London, 1993.

Kline, M., and Kay, I. W., *Electromagnetic Theory and Geometrical Optics*, John Wiley and Sons, New York, 1965.

Karal, F. C., and J. B. Keller, Elastic wave propagation in homogeneous and inhomogeneous media, *Journal of the Acoustical Society of America, 31*, 694-705, 1959.

Karasaki, K., B. Freifeld, A. Cohen, K. Grossenbacher, P. Cook, and D. Vasco, A multi-disciplinary fractured rock characterization study at the Raymond field site, California *Journal of Hydrology*, 236, 17-34, 2000.

Kowalsky, M. B., S. Finsterle, and Y. Rubin, Estimating flow parameter distributions using ground-penetrating radar and hydrological measurements during transient flow in the vadose zone, *Advances in Water Resources*, **27**, 583-599, 2004.

Kowalsky, M. B., S. Finsterle, J. Peterson, S. Hubbard, Y. Rubin, E. Majer, A. Ward, and G. Gee, Estimation of field-scale soil hydraulic and dielectric parameters through joint inversion of GPR and hydrological data, *Water Resources Research*, **41**, W011425, doi:10.1029/2005WR004237,2005.

Kravtsov, Y. A., and Y. I. Orlov, *Geometrical Optics of Inhomogeneous Media*, Springer-Verlag, Berlin, 1990.

Lanczos, C., *The Variational Principles of Mechanics*, Dover Publications, New York, 1986.

Lecomte, I., Finite difference calculation of first traveltimes in anisotropic media, *Geophysical Journal International*, **113**, 318-342, 1993.

Luneburg, R. K., *Mathematical Theory of Optics*, University of California Press, Berkeley, 1966.

Maslov, V. P., and G. A. Omel'yanov, *Geometric Asymptotics for Nonlinear PDE. I*, American Mathematical Society, Providence, Rhode Island, 2001.

Noble, B., and Daniel, J. W., *Applied Linear Algebra*, Prentice-Hall, Englewood Cliffs, 1977.

Paillet, F. L., Using borehole geophysics and cross-borehole flow testing to define connections between fracture zones in bedrock aquifers, *Journal of Applied Geophysics*, **30**, 261-279, 1993.

Peaceman, D., W., *Fundamentals of Numerical Reservoir Simulation*, Elesevier Scientific Publishing, Amsterdam, 1977.

Press, W. H., S. A. Teukolsky, W. T. Vetterling, and B. P. Flannery, *Numerical Recipes*, Cambridge University Press, Cambridge, 1992.

Pruess, K., C. Oldenburg, and G. Moridis, *TOUGH2 User's Guide, Version 2.0*, LBNL Report, **43134**, Berkeley, 1999.

Qian, J., and Symes, W. W., Paraxial eikonal solvers for anisotropic quasi-P travel times, *Journal of Computational Physics*, **173**, 256-278, 2001.

Rucci, A., D. W. Vasco, and F. Novali, Fluid pressure arrival time tomography: Estimation and assessment in the presence of inequality constraints, with an application to a producing gas field at Krechba, Algeria, *Geophysics*, (in press), 2010.

Schmidt, D. A., and R. Burgmann, Time-dependent land uplift and subsidence in the Santa Clara valley, California, from a large interferometric synthetic aperture radar data set, *Journal of Geophysical Research*, **108**, 4-1-4-13, doi:10.1029/2002JB002267, 2003.

Sethian, J. A., Numerical algorithms for propagating interfaces: Hamilton-Jacobi equations and conservation laws, *Journal of Differential Geometry*, **31**, 131-161, 1990.

Sethian, J. A., *Level Set Methods*, Cambridge University Press, 1999.

Sethian, J. A., and J. D. Strain, Crystal growth and dendritic solidification, *Journal of Computational Physics*, **98**, 231-253, 1992.

Shen, M. C., Ray method for flow of a compressible viscous fluid, *SIAM Journal of Applied Mathematics*, **43**, 822-833, 1983.

Sneddon, I. N., *Elements of Partial Differential Equations*, Dover Publications, New York, 2006.

Soukina, S. M., D. Gajewski, and B. M. Kashtan, Traveltime computation for 3D anisotropic media by a finite-difference perturbation method, *Geophysical Prospecting*, **51**, 431-441, 2003.

Sturmfels, B., *Solving Systems of Polynomial Equations*, American Mathematical Society, Providence, RI, 2002.

Sun, N. -Z., *Inverse Problems in Groundwater Modeling*, Kluwer Academic Press, Norwell, MA, 1994.

Tuncay, K., and M. Y. Corapcioglu, Body waves in poroelastic media saturated by two immiscible fluids, *Journal of Geophysical Research*, **101**, 25149-25159, 1996.

van Trier, J., and W. W. Symes, Upwind finite-difference calculations of traveltimes, *Geophysics*, **56**, 812-821, 1991.

Vasco, D. W., An asymptotic solution for two-phase flow in the presence of capillary forces, *Water Resources Research*, **40**, W12407, 2004.

Vasco, D. W., Zeroth-order inversion of transient pressure observations, *Inverse Problems*, **24**, 1-21, doi:10.1088/0266-5611/24/2/025013, 2008a.

Vasco, D. W., Trajectory-based methods for modeling and characterization, in *Quantitative Information Fusion for Hydrological Sciences*, Xing, C., and Yeh, T. -C. J. (eds) Springer-Verlag, Studies in Computational Intelligence, 69-103, 2008b.

Vasco, D. W., and A. Datta-Gupta, Asymptotic solutions for solute transport: A formalism for tracer tomography, *Water Resources Research*, **35**, 1-16, 1999.

Vasco, D. W., and Finsterle, S., Numerical trajectory calculations for the efficient inversion of flow and tracer observations, *Water Resources Research*, **40**, W01507, 1-17, 2004.

Vasco, D. W., S. Yoon, and A. Datta-Gupta, Integrating dynamic data into high-resolution reservoir models using streamline-based analytic sensitivity coefficients, *SPE Journal*, *4*, 389-399, 1999.

Vasco, D. W., H. Keers, and K. Karasaki, Estimation of reservoir properties using transient pressure data: An asymptotic approach, *Water Resources Research, 36*, 3447-3465, 2000.

Vasco, D. W., A. Rucci, A. Ferretti, F. Novali, R. C. Bissell, P. S. Ringrose, A. S. Mathieson, and I. W., Wright, Satellite-based measurements of surface deformation reveal fluid flow associated with the geological storage of carbon dioxide, *Geophysical Research Letters, 37*, L03303, doi:10.1029/2009/GL041544, 2010.

Vesselinov, V. V., S. P. Neuman, and W. A. Illmin, Three-dimensional numerical inversion of pneumatic cross-hole tests in unsaturated fractured tuff: 2. Equivalent parameters, high-resolution stochastic imagin, and scale effects, *Water Resources Research*, **37**, 3001-3017, 2001.

Vidale, J., Finite-difference calculation of travel times, *Bulletin of the Seismological Society of America, 78*, 2062-2076, 1988.

Virieux, J., C. Flores-Luna, and D. Gibert, Asymptotic theory for diffusive electromagnetic imaging, *Geophysical Journal International*, **119**, 857-868, 1994.

Whitham, G. B., *Linear and Nonlinear Waves*, John Wiley and Sons, New York, 1974.

Yeh, T. C., and S. Liu, Hydraulic tomography: Development of a new aquifer test method, *Water Resources Research*, **36**, 2095-2105, 2000.

D. W. Vasco, Earth Sciences Division/Building 90, Berkeley Laboratory, 1 Cyclotron Road, Berkeley, CA 94720. (e-mail:dwvasco@lbl.gov)

7. Figure Captions

Figure 1. The relative permeability curves for the non-aqueous phase liquid (NAPL) and for water as a function of the water saturation. The non-aqueous phase liquid function is the default for oil in the reservoir simulator TOUGH2 [*Pruess et al.*, 1999].

Figure 2. (A) The distribution of water saturation in the porous layer after 100 days of water injection. The two observation points are denoted by the filled and open circles. (B) The pressure field after 100 days of injection.

Figure 3. (A) The time varying saturation change at the first observation point [indicated by the filled circle in Figure 2]. (B) The time varying pressure at the first observation point.

Figure 4. (A) The time derivative of the saturation change. (B) the time derivative of the pressure variation at the first observation point.

Figure 5. The normalized time derivatives of the saturation and pressure variations for the first 150 days since the start of the water injection. The derivatives are normalized such that the peak values are 1.

Figure 6. Snapshots of the normalized time derivative of the saturation variation for three different times. The time derivative of the saturation variation in each grid block is formed and normalized such that its peak value is one.

Figure 7. Snapshots of the normalized time derivatives of the pressure variation for three different times. The time derivative of the pressure variation in each grid block is formed and normalized such that its peak value is one.

Figure 8. Contour plots of the phase function computed from the saturation and pressure variations in each block of the simulation grid. The two observation points are signified by the filled and unfilled circles. Trajectories, extending from the second observation point to the injection well, are denoted by the solid lines.

Figure 9. Travel times associated with various points along the trajectories shown in Figure 8, which extends from the second observation point to the injection well. The travel times for the saturation and pressure phase functions are associated with the time at which the derivative attains its maximum value. The travel times calculated using the asymptotic expression [see equation (75)] are also plotted for points along the trajectory.

Figure 10. The time derivatives of the saturation and pressure variations at the first observation point [denoted by a filled circle in Figure 1]. The derivatives have been normalized such that the peak values are 1. The values are associated with the second set of peaks, between 200 and 400 seconds, in Figure 4. A background pressure variation, calculated for oil injection in an oil saturated layer, has been removed from the pressure curve.

Figure 11. Snapshots of the normalized time derivatives of the saturation variation in each grid block.

Figure 12. Snapshots of the normalized time derivatives of the pressure variation in each grid block. A background pressure variation, calculated for oil injection in an oil saturated layer, has been removed from the pressure curve in each grid block.

Figure 13. Contour plots of the phase function computed from the saturation and pressure variations in each block of the simulation grid. The phase functions correspond to the second set of peaks in Figure 4, the second arrival. The two observation points are signified by the filled and unfilled circles. Trajectories, extending from the second observation point to the injection well, are denoted by the solid lines.

Figure 14. Travel time to points at various distances along the trajectories plotted in Figure 13. The saturation and pressure estimates were obtained by post-processing the output of the numerical simulator TOUGH2 [*Pruess et al.*, 1999). The asymptotic estimates, based upon Ω given by (76), are denoted by the crosses.

Figure 15. Permeability model used in the heterogeneous test case. The darker colors denote higher permeability. Two observation points are indicated by the filled and unfilled circles. The injection well is denoted by the star and the trajectory is a curve connecting the outermost observation point with the injection well.

Figure 16. (A) The distribution of water saturation in the heterogeneous porous layer after 525 days of water injection. The two observation points are denoted by the filled and open circles. (B) The pressure field after 525 days of injection.

Figure 17. (A) The time derivative of the saturation change. (B) the time derivative of the pressure variation at the first observation point.

Figure 18. Contour plots of the phase function computed from the saturation and pressure variations in each block of the simulation grid. The two observation points are signified by the filled and unfilled circles. Trajectories, extending from the second observation point to the injection well, are denoted by the solid lines.

Figure 19. Travel times associated with various points along the trajectories shown in Figure 18, which extends from the second observation point to the injection well. The travel times for the saturation and pressure phase functions are associated with the time at which the derivative attains its maximum value. The travel times calculated using the asymptotic expression [see equation (76)] are also plotted for points along the trajectory.

Figure 20. Contour plots of the phase function computed from the saturation variations in each block of the simulation grid. The phase function corresponds to the second peak in Figure 17, the second arrival. The two observation points are signified by the filled and unfilled circles. A trajectory, extending from the second observation point to the injection well, is denoted by the solid line.

Figure 21. Travel times associated with various points along the trajectory shown in Figure 20, which extends from the second observation point to the injection well. The travel times for the saturation phase function is associated with the time at which the derivative attains its maximum value. The travel times calculated using the asymptotic slowness expression [see equation (76)] are also plotted for points along the trajectory.

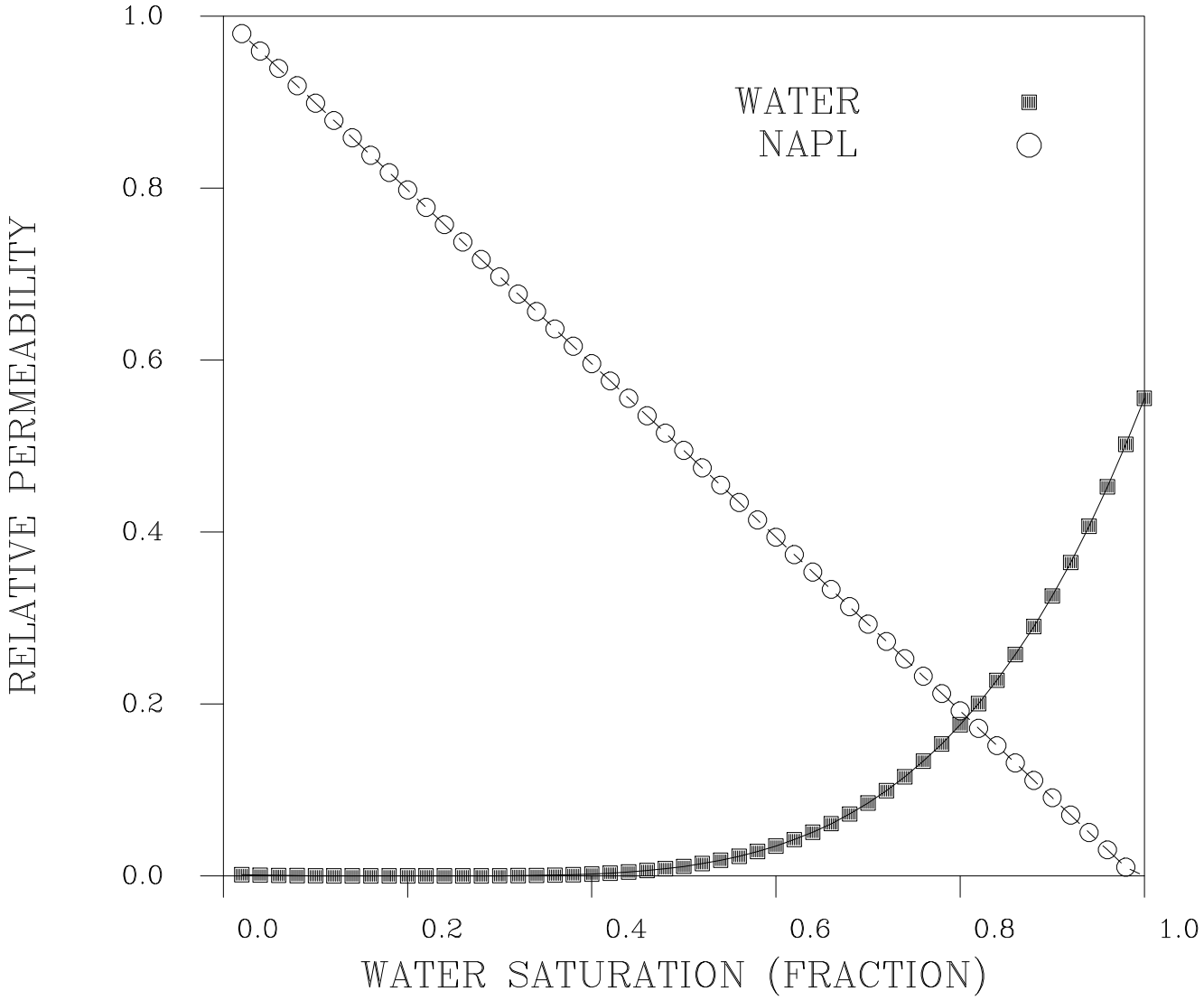
RELATIVE PERMEABILITY
1.0
0.8
0.6
0.4
0.2
0.0
WATER
NAPL
0.0
0.2
0.4
0.6
0.8
1.0
WATER SATURATION (FRACTION)

Figure 1.

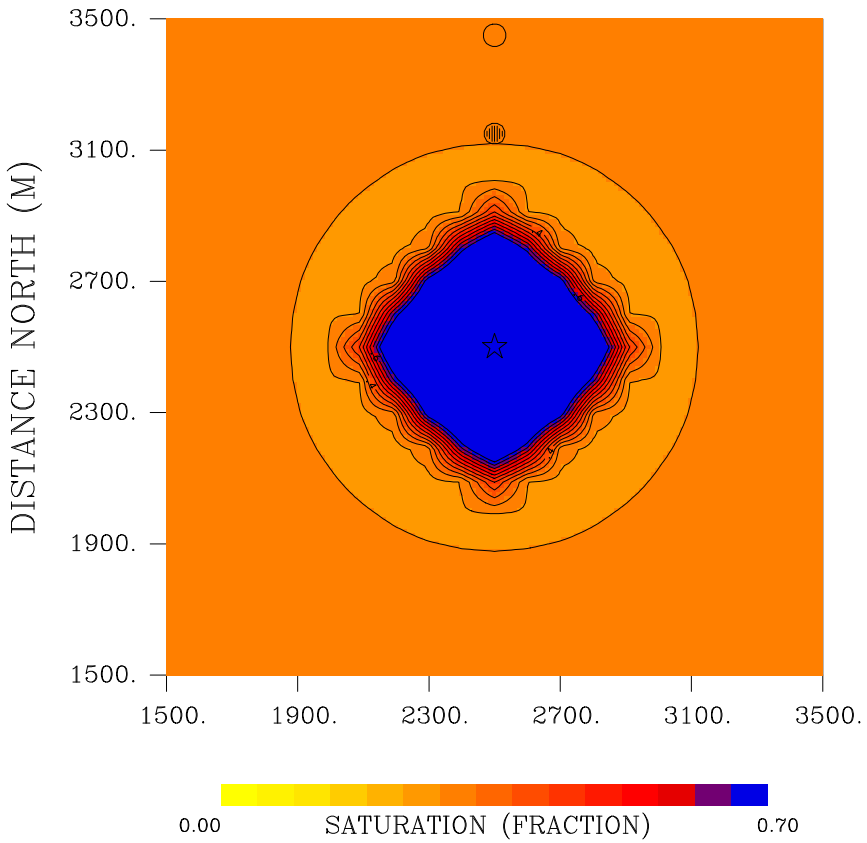
3500.
3100.
2700.
2300.
1900.
1500.
DISTANCE NORTH (M)
1500.
1900.
2300.
2700.
3100.
3500.
0.00
SATURATION (FRACTION)
0.70

A.

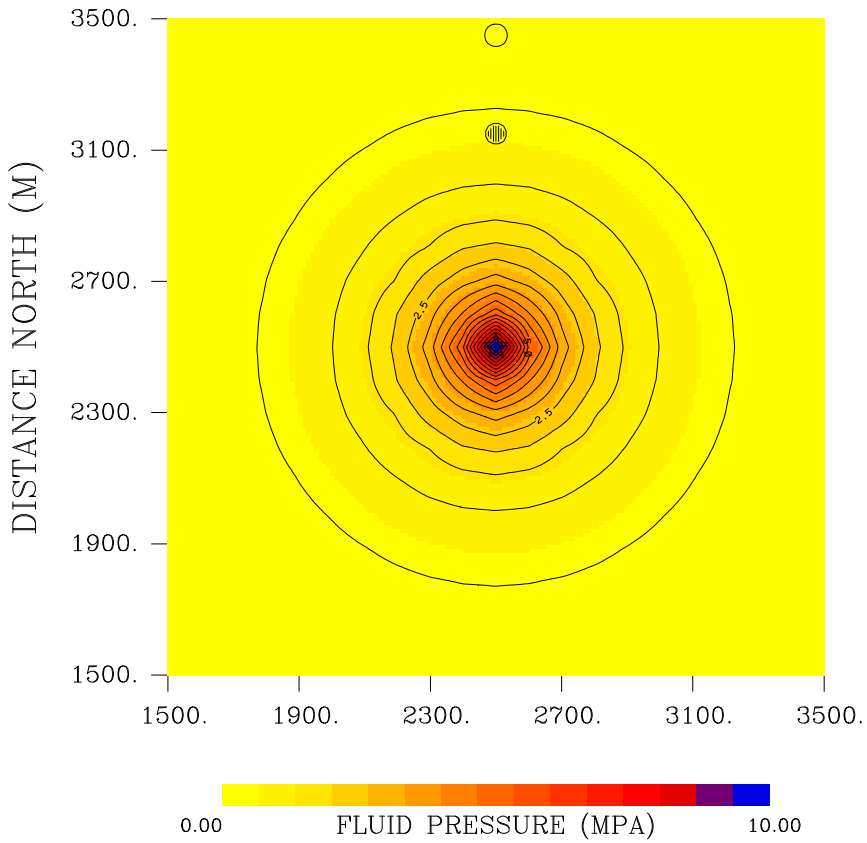
3500.
3100.
2700.
2300.
1900.
1500.
DISTANCE NORTH (M)
1500.
1900.
2300.
2700.
3100.
3500.
0.00
FLUID PRESSURE (MPA)
10.00

B.

Figure 2.

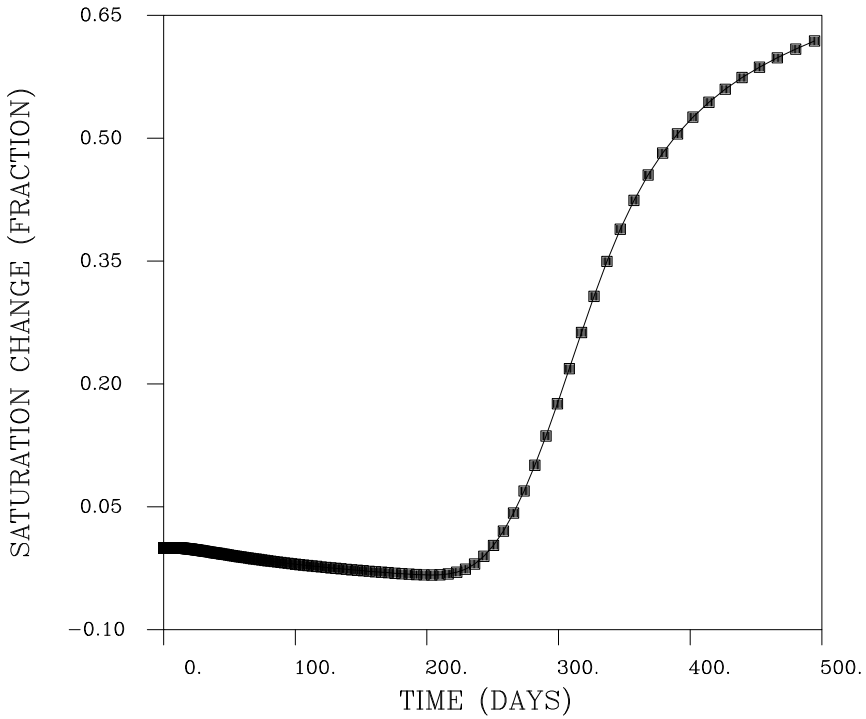
SATURATION CHANGE (FRACTION)
0.65
0.50
0.35
0.20
0.05
−0.10
0.
100.
200.
300.
400.
500.
TIME (DAYS)

A.

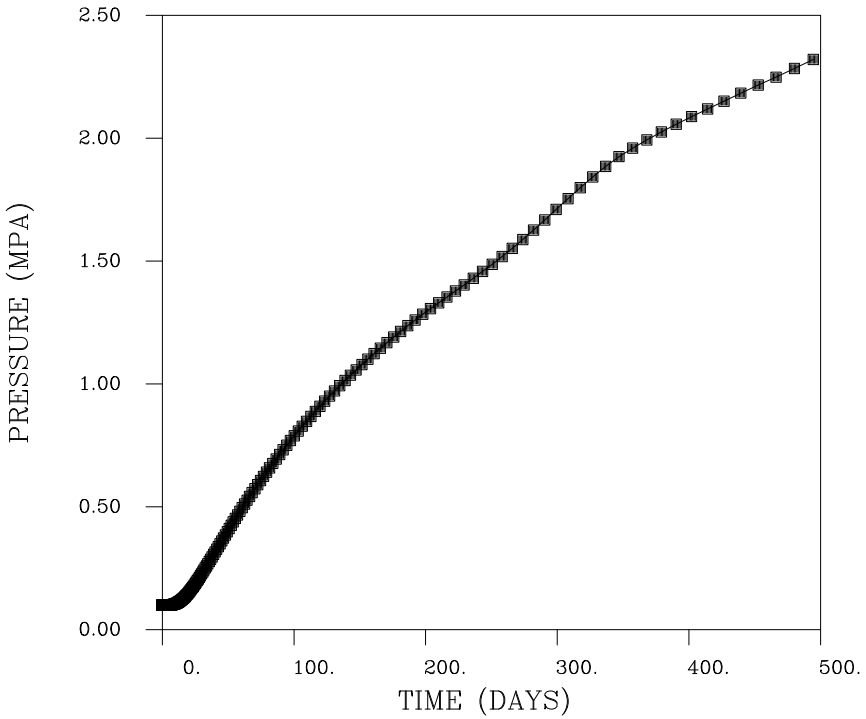
PRESSURE (MPA)
2.50
2.00
1.50
1.00
0.50
0.00
0.
100.
200.
300.
400.
500.
TIME (DAYS)

B.

Figure 3.

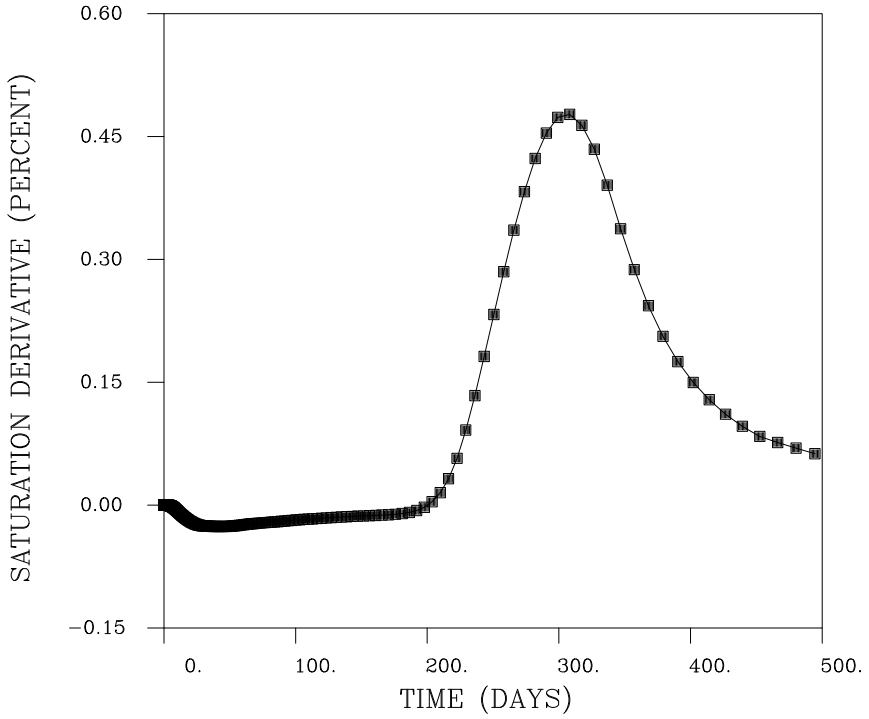
SATURATION DERIVATIVE (PERCENT)
0.60
0.45
0.30
0.15
0.00
−0.15
0.
100.
200.
300.
400.
500.
TIME (DAYS)

A.

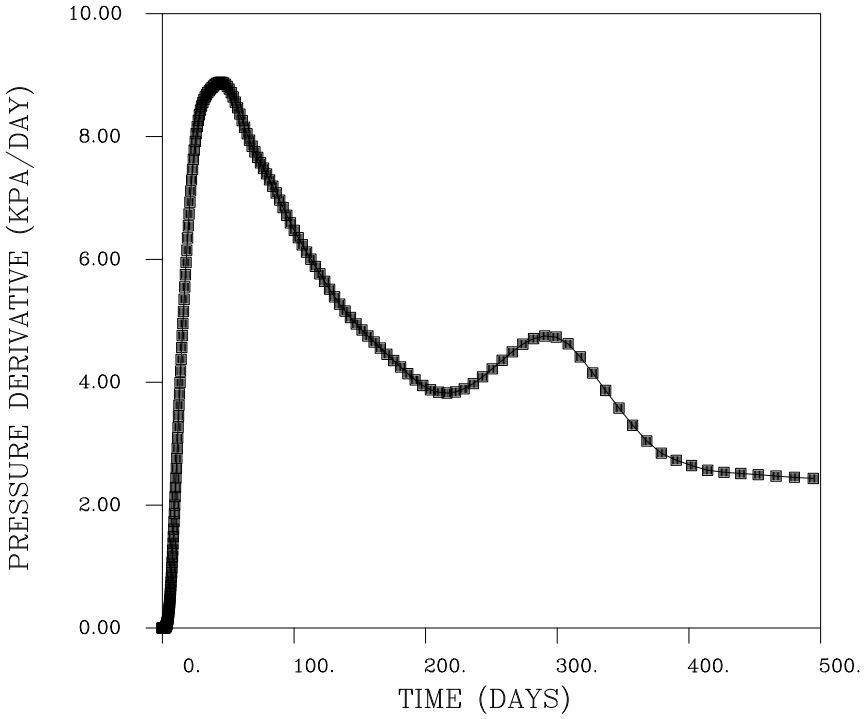
PRESSURE DERIVATIVE (KPA/DAY)
10.00
8.00
6.00
4.00
2.00
0.00
0.
100.
200.
300.
400.
500.
TIME (DAYS)

B.

Figure 4.

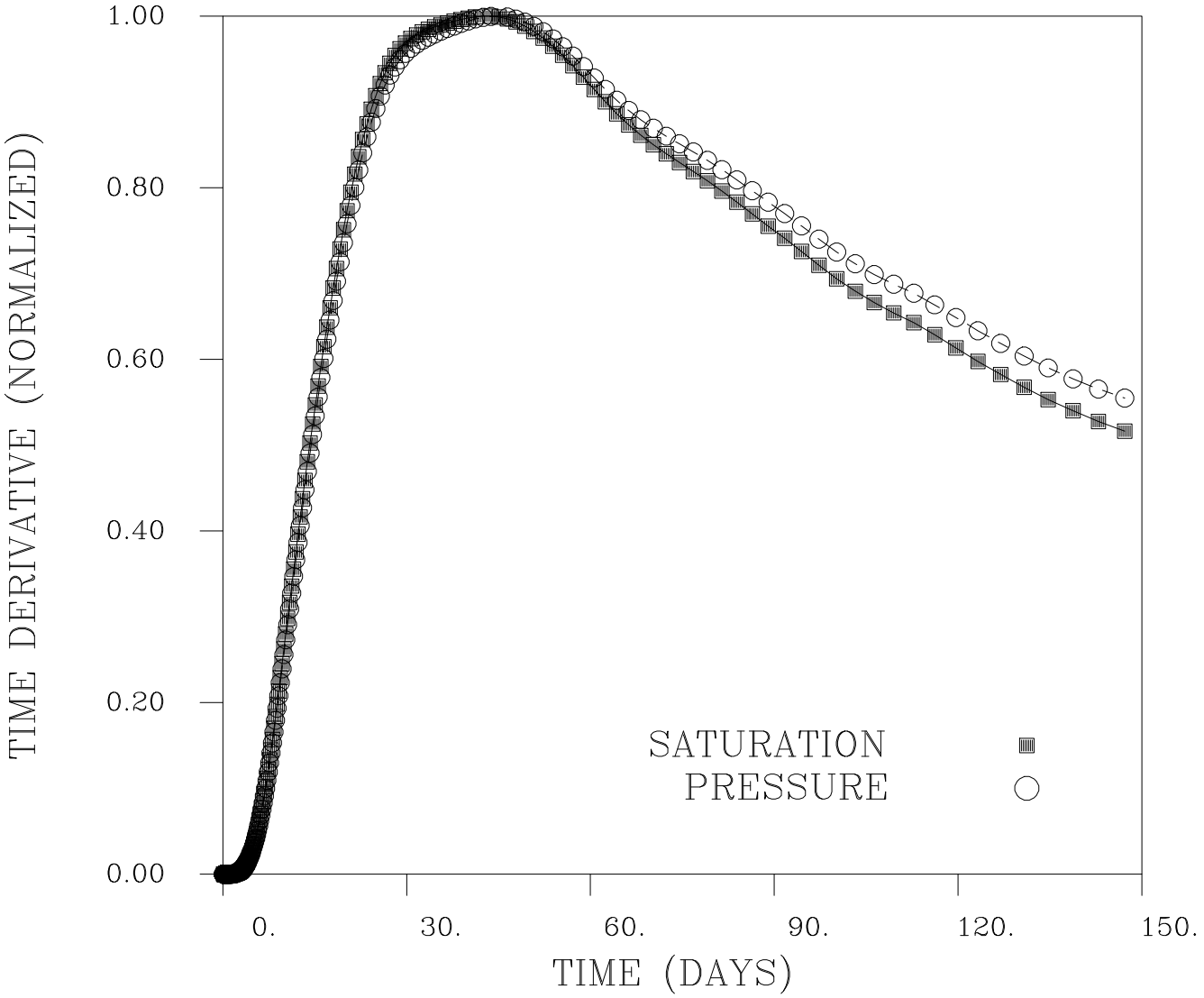
1.00
0.80
0.60
0.40
0.20
0.00
TIME DERIVATIVE (NORMALIZED)
SATURATION
PRESSURE
0.
30.
60.
90.
120.
150.
TIME (DAYS)

Figure 5.

Saturation

30 Days

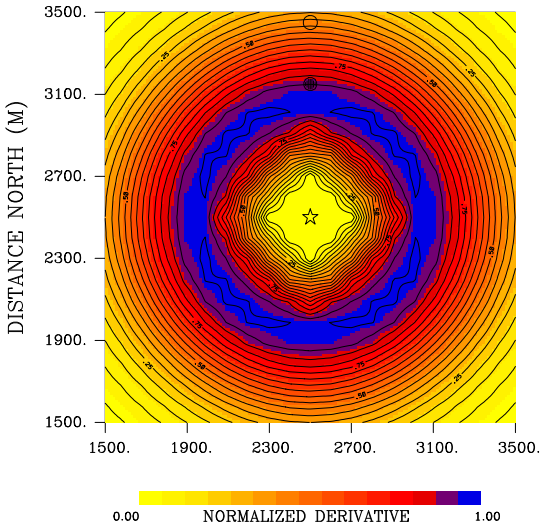

60 Days

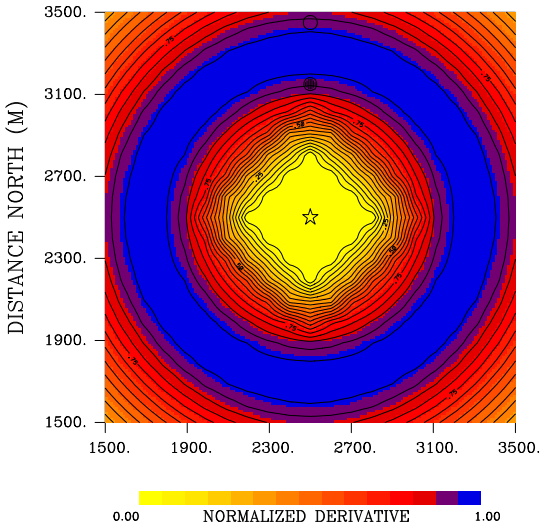

120 Days

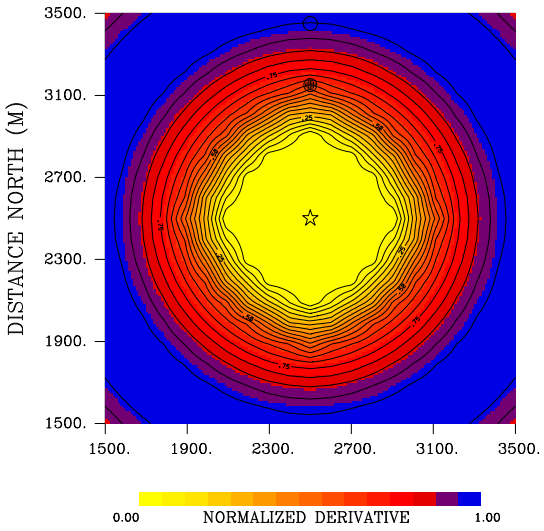

Figure 6.

Pressure

30 Days

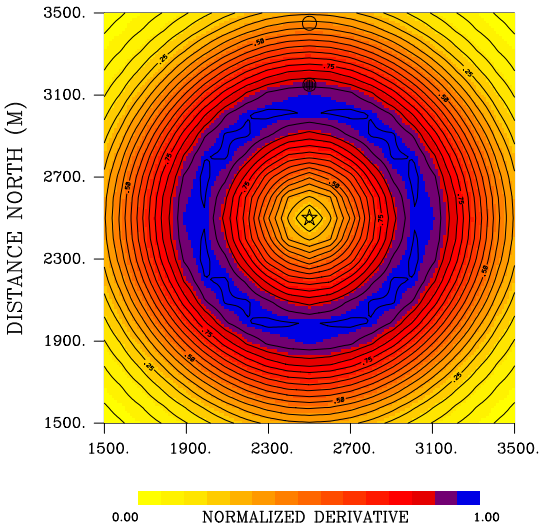

60 Days

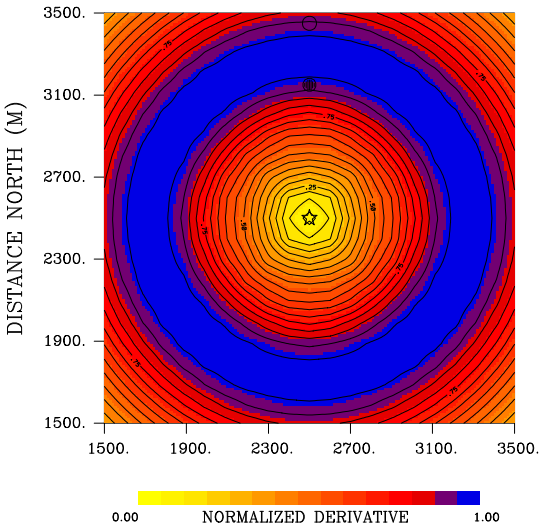

120 Days

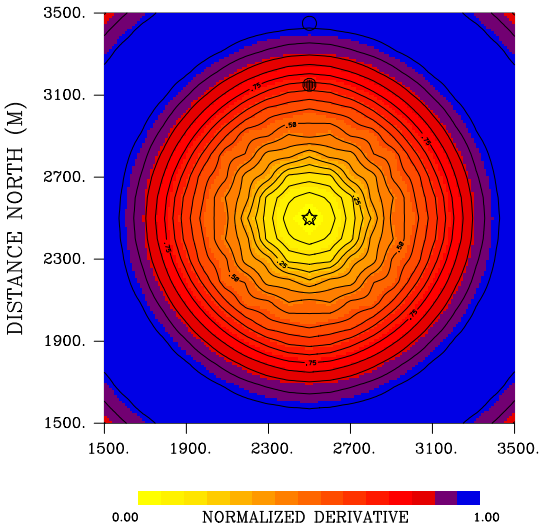

Figure 7.

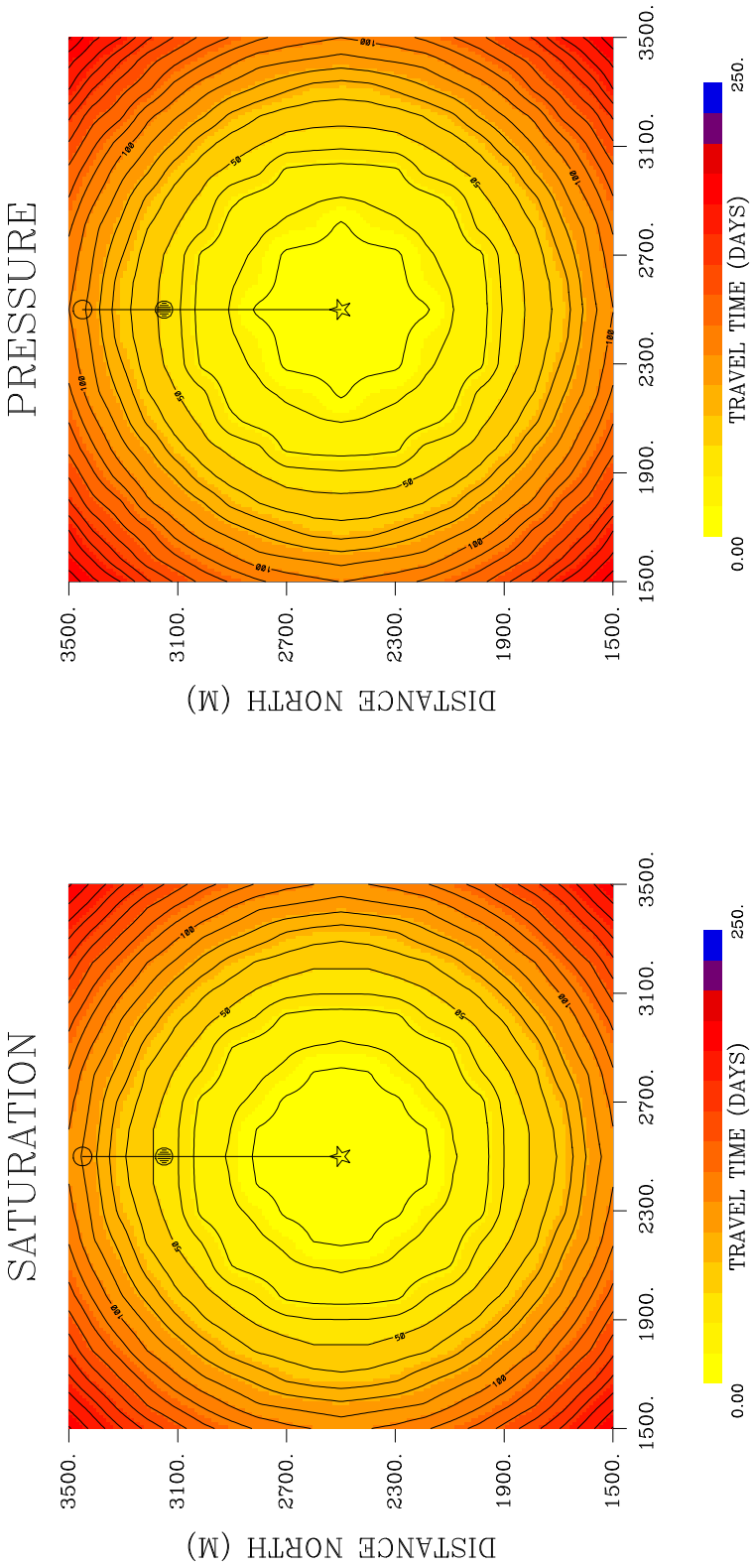
PRESSURE
SATURATION
DISTANCE NORTH (M)
3500.
3100.
2700.
2300.
1900.
1500.
TRAVEL TIME (DAYS)
0.00
250.

Figure 8.

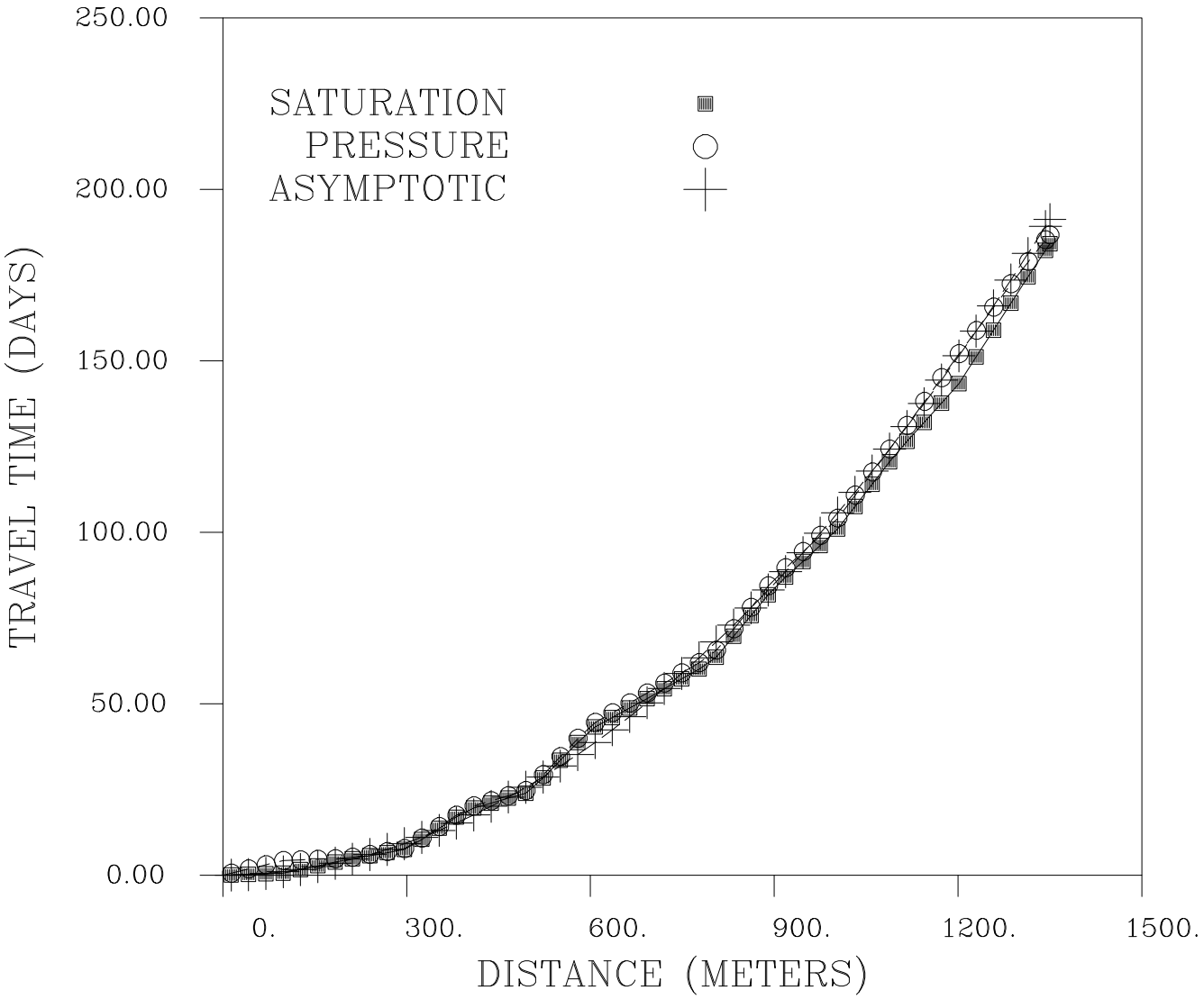
250.00
200.00
150.00
100.00
50.00
0.00
TRAVEL TIME (DAYS)
SATURATION
PRESSURE
ASYMPTOTIC
0.
300.
600.
900.
1200.
1500.
DISTANCE (METERS)

Figure 9.

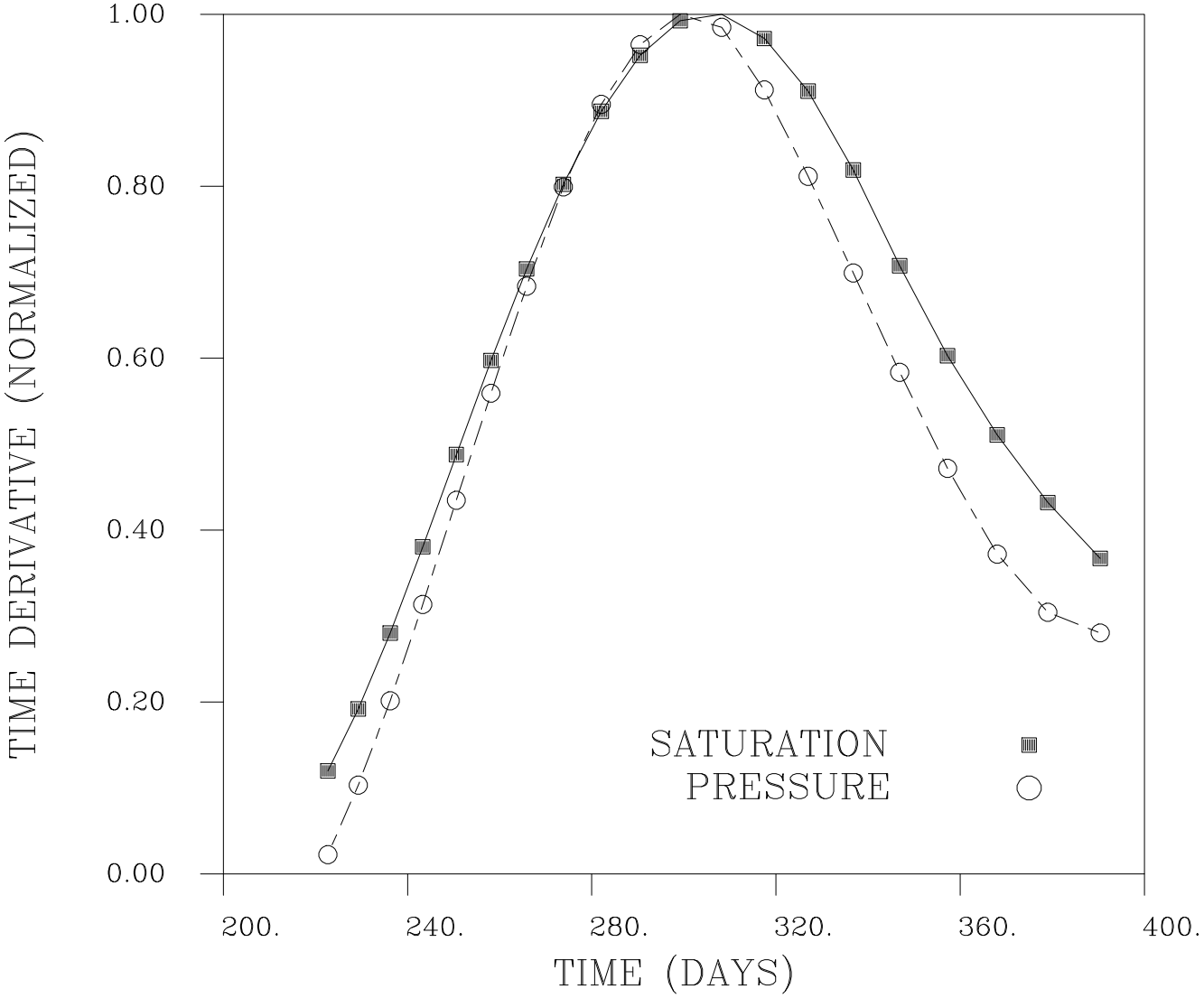
TIME DERIVATIVE (NORMALIZED)
1.00
0.80
0.60
0.40
0.20
0.00
200.
240.
280.
320.
360.
400.
TIME (DAYS)
SATURATION
PRESSURE

Figure 10.

Saturation

299 Days

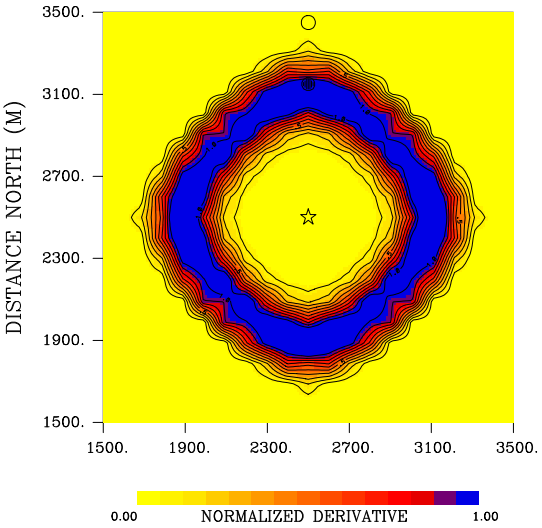

525 Days

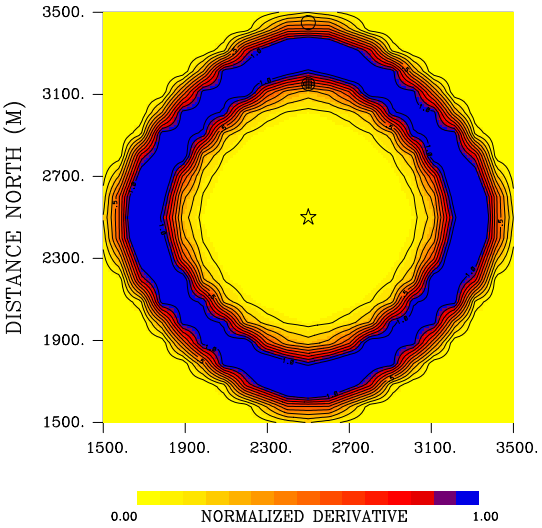

1005 Days

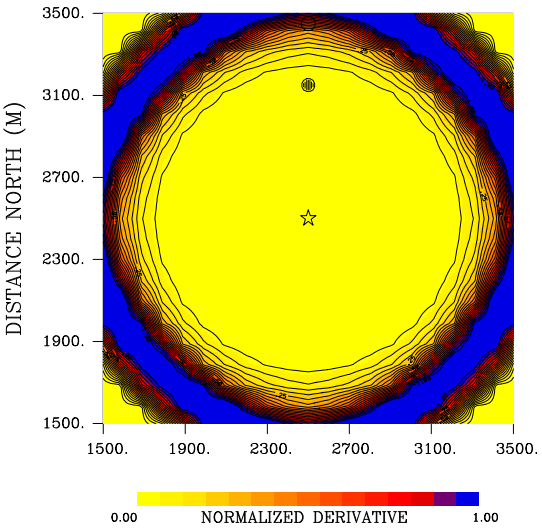

Figure 11.

Pressure

299 Days

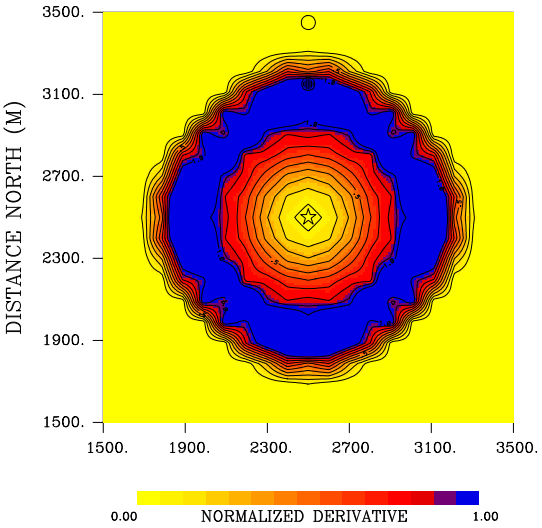

525 Days

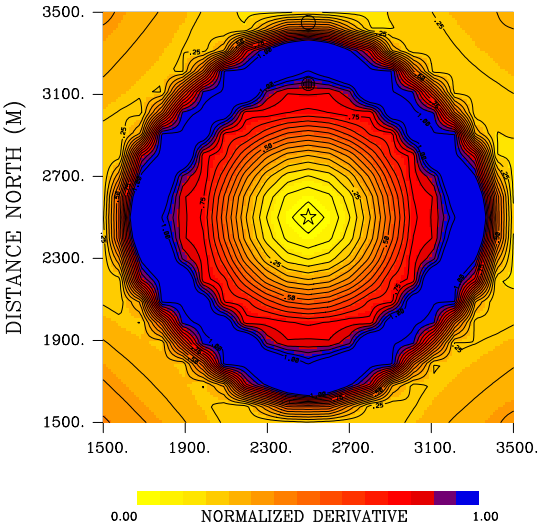

1005 Days

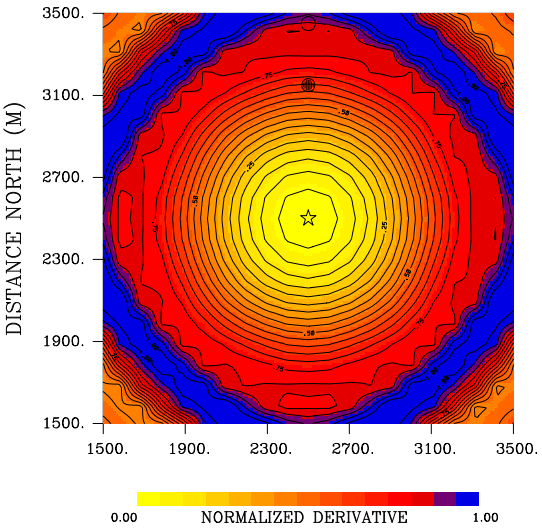

Figure 12.

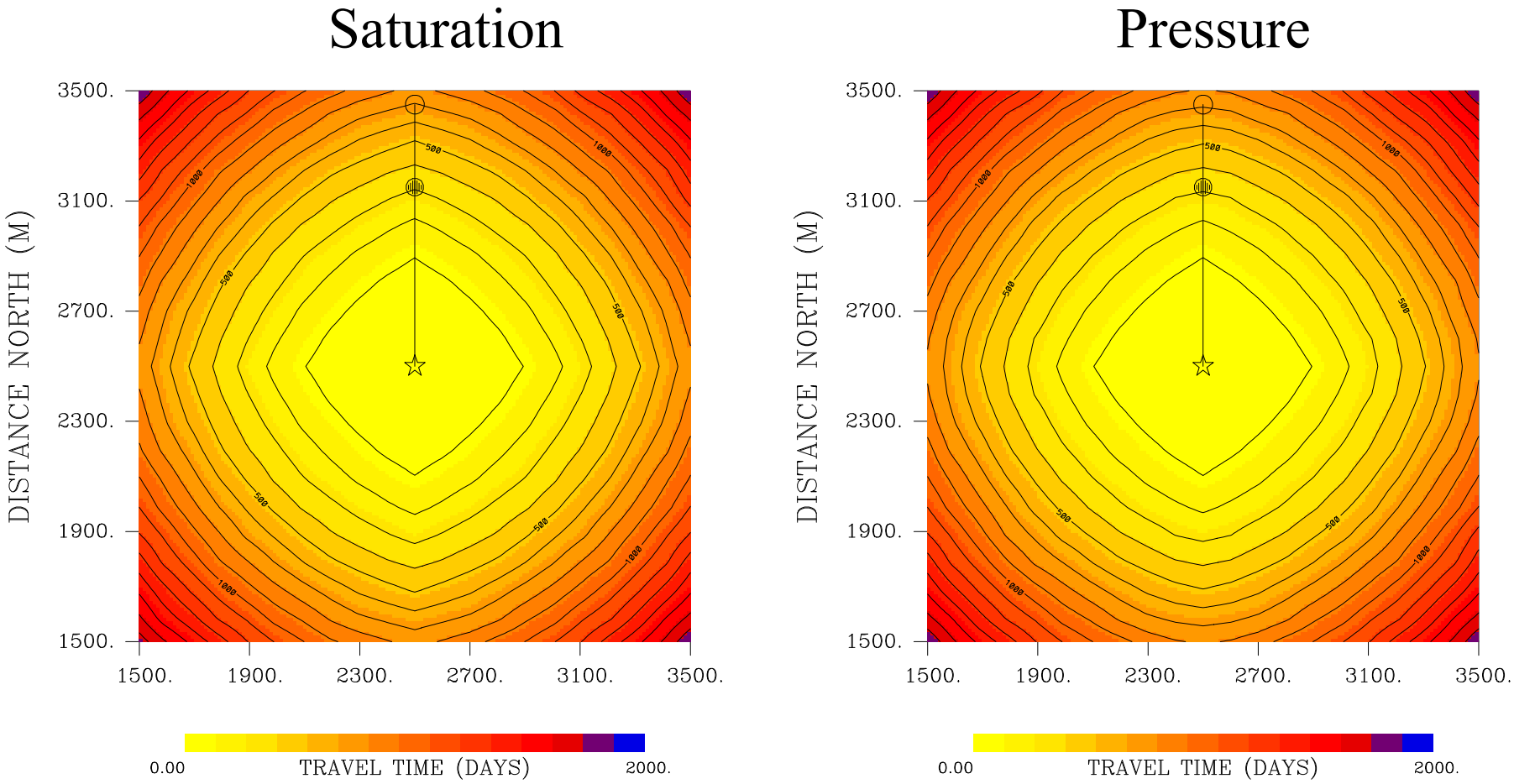
Saturation
Pressure
DISTANCE NORTH (M)
3500.
3100.
2700.
2300.
1900.
1500.
500
1000
0.00
TRAVEL TIME (DAYS)
2000.
A.
B.

Figure 13.

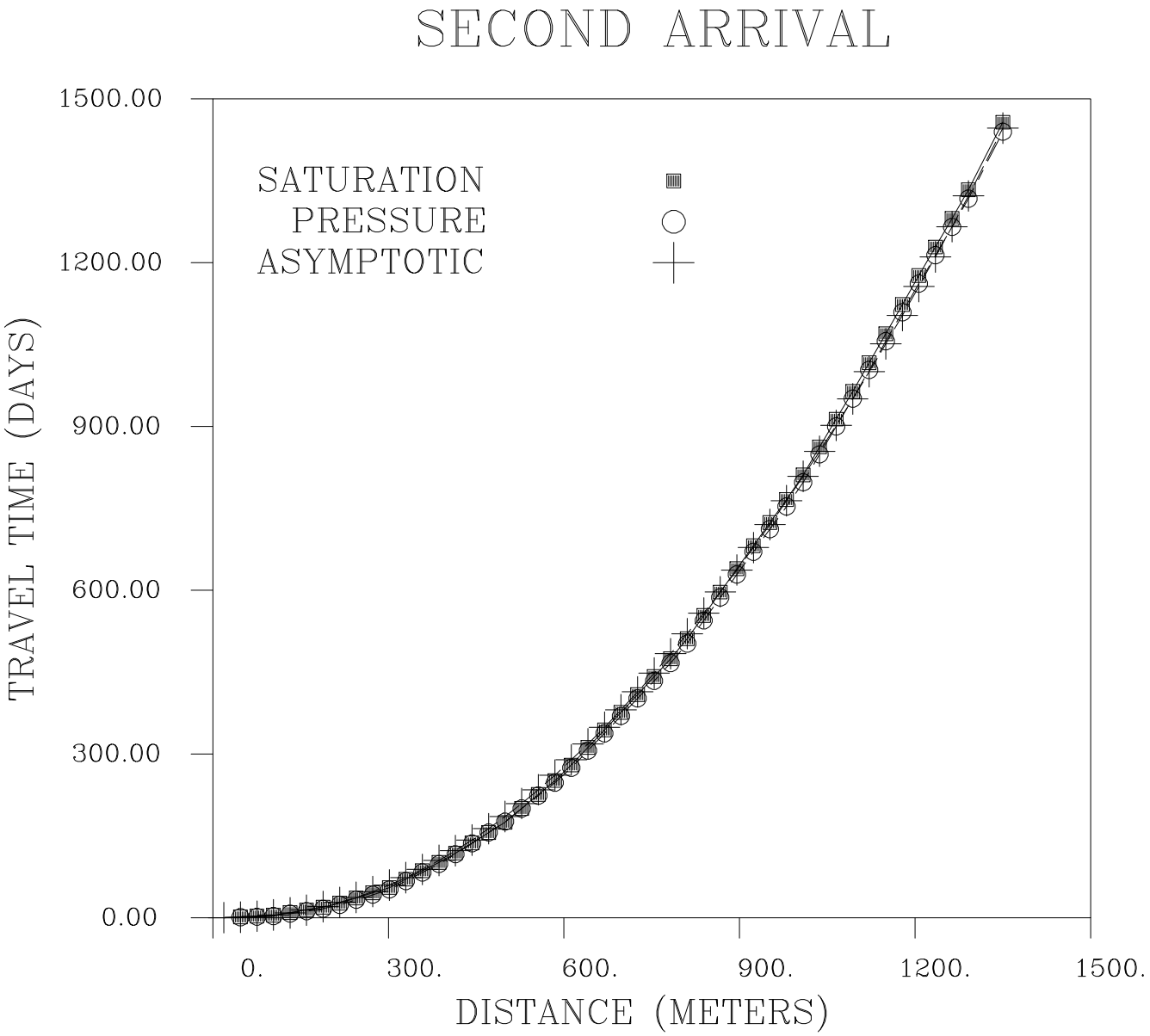
SECOND ARRIVAL
SATURATION
PRESSURE
ASYMPTOTIC
TRAVEL TIME (DAYS)
1500.00
1200.00
900.00
600.00
300.00
0.00
0.
300.
600.
900.
1200.
1500.
DISTANCE (METERS)

Figure 14.

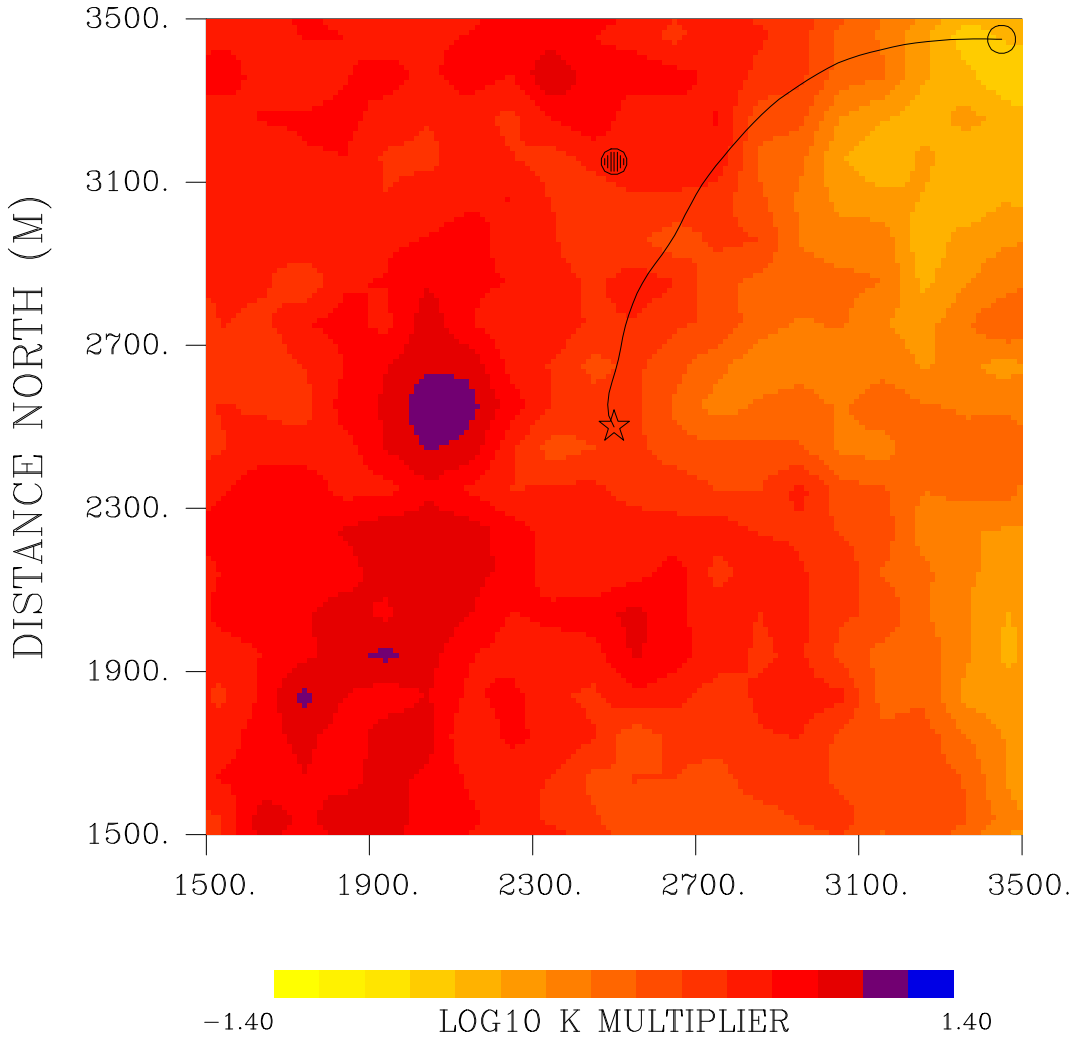
3500.
3100.
2700.
2300.
1900.
1500.
DISTANCE NORTH (M)
1500.
1900.
2300.
2700.
3100.
3500.
−1.40
LOG10 K MULTIPLIER
1.40

Figure 15.

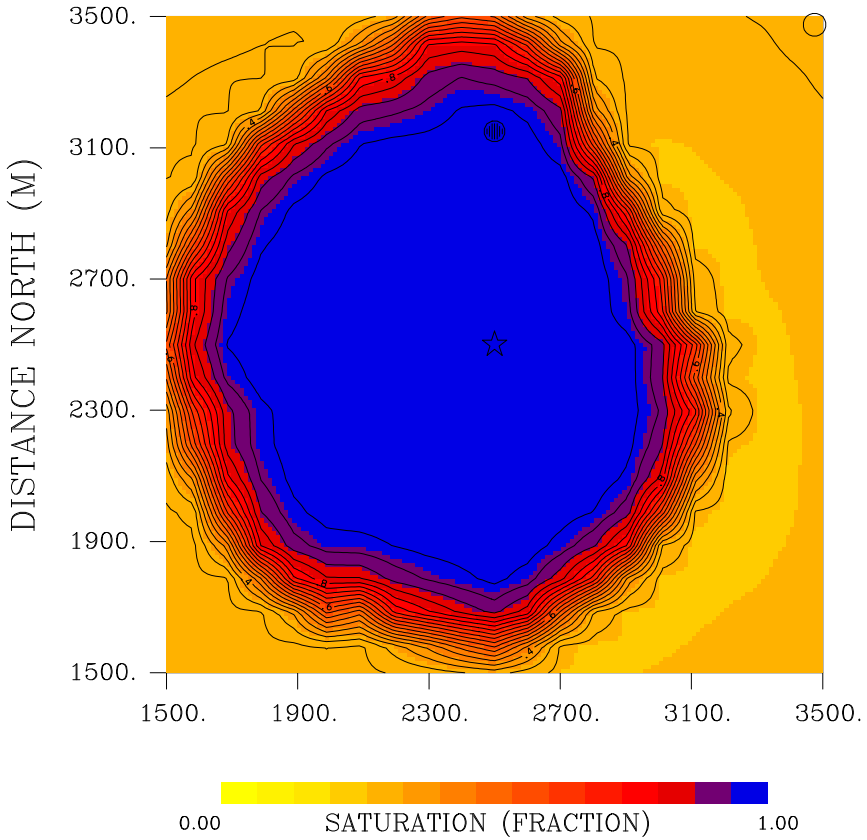
3500.
3100.
2700.
2300.
1900.
1500.
DISTANCE NORTH (M)
1500.
1900.
2300.
2700.
3100.
3500.
0.00
SATURATION (FRACTION)
1.00

A.

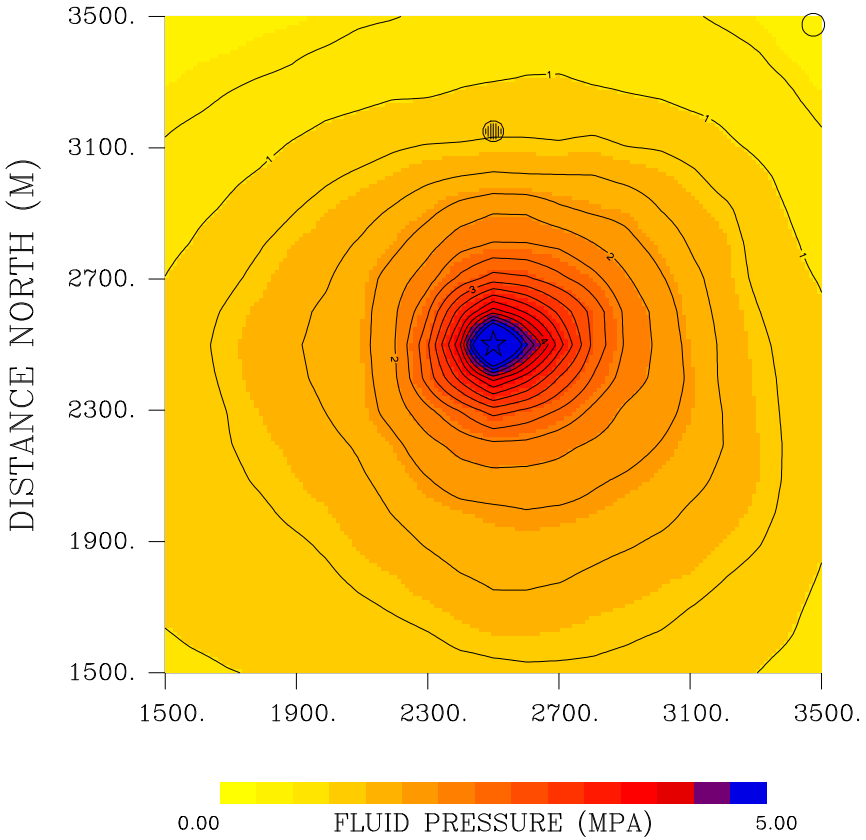
3500.
3100.
2700.
2300.
1900.
1500.
DISTANCE NORTH (M)
1500.
1900.
2300.
2700.
3100.
3500.
0.00
FLUID PRESSURE (MPA)
5.00

B.

Figure 16.

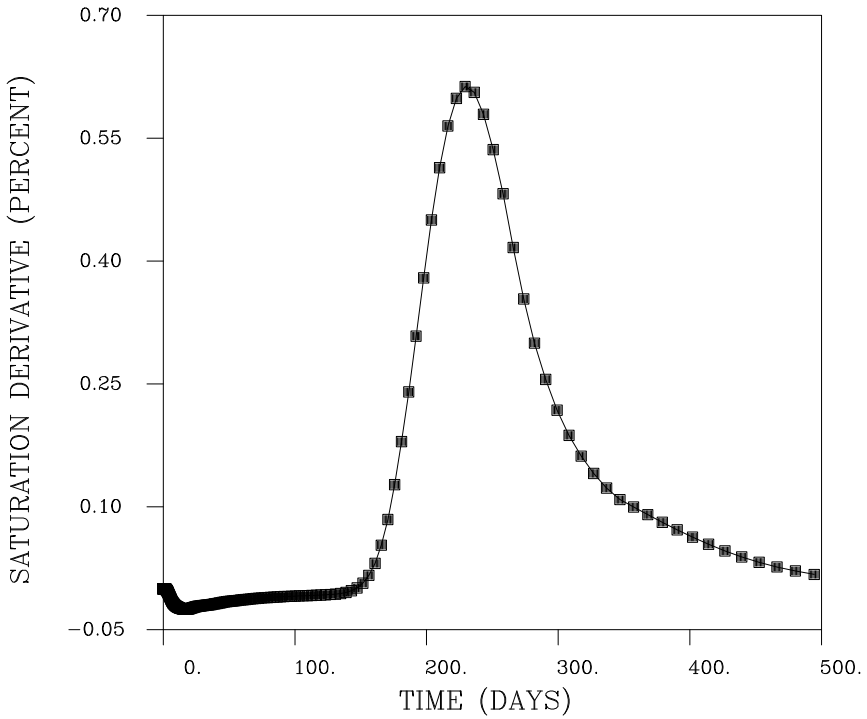
SATURATION DERIVATIVE (PERCENT)
0.70
0.55
0.40
0.25
0.10
−0.05
0.
100.
200.
300.
400.
500.
TIME (DAYS)

A.

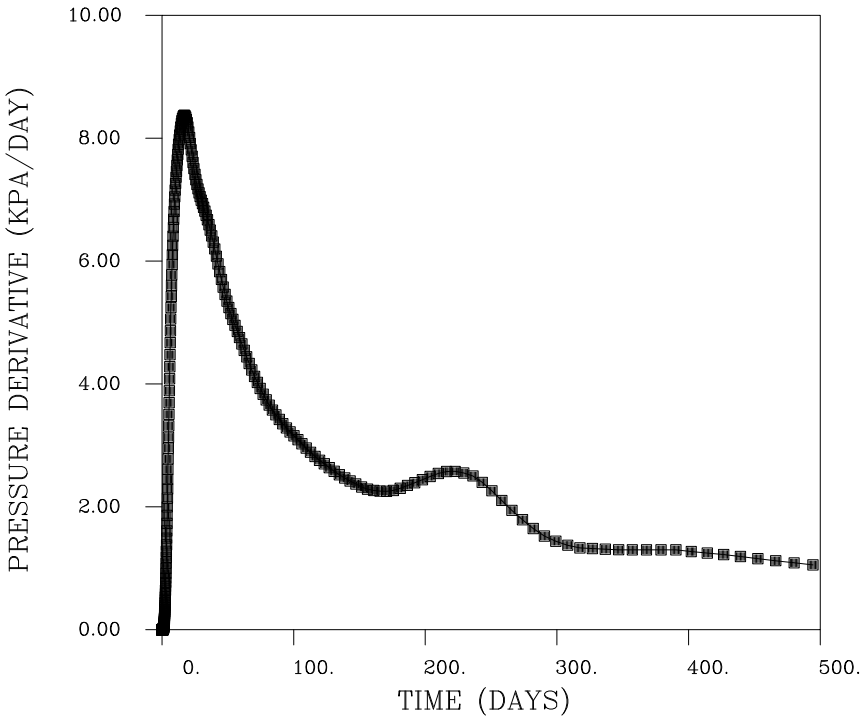
PRESSURE DERIVATIVE (KPA/DAY)
10.00
8.00
6.00
4.00
2.00
0.00
0.
100.
200.
300.
400.
500.
TIME (DAYS)

B

Figure 17.

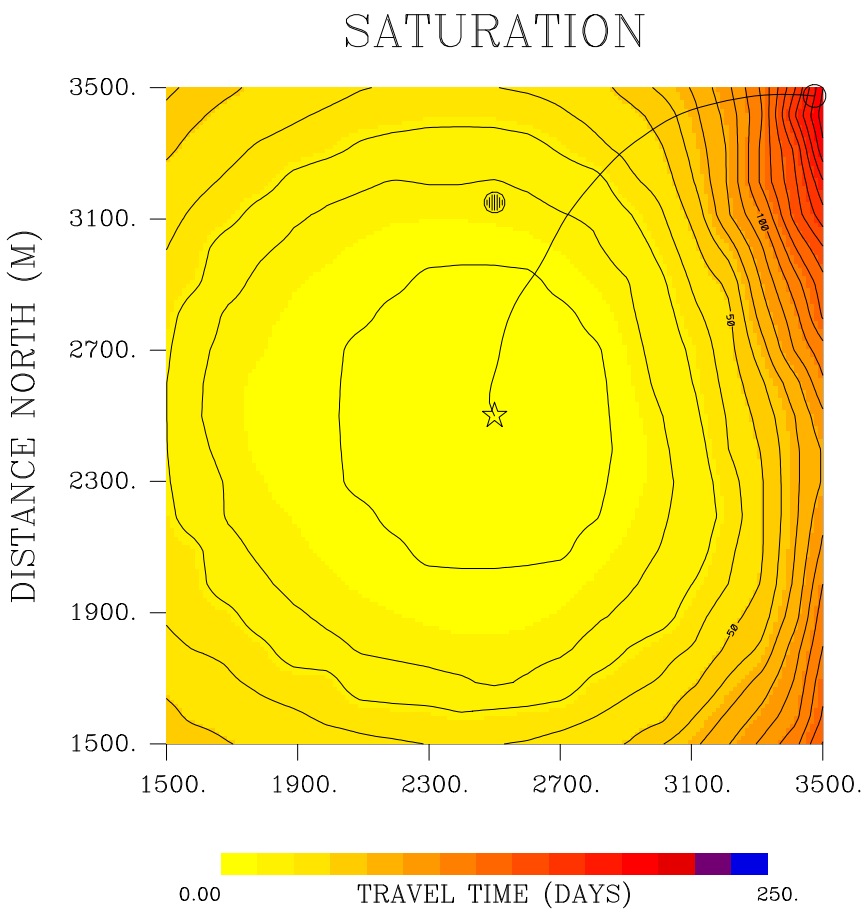
SATURATION
DISTANCE NORTH (M)
3500.
3100.
2700.
2300.
1900.
1500.
1500.
1900.
2300.
2700.
3100.
3500.
100
50
50
0.00
TRAVEL TIME (DAYS)
250.

A.

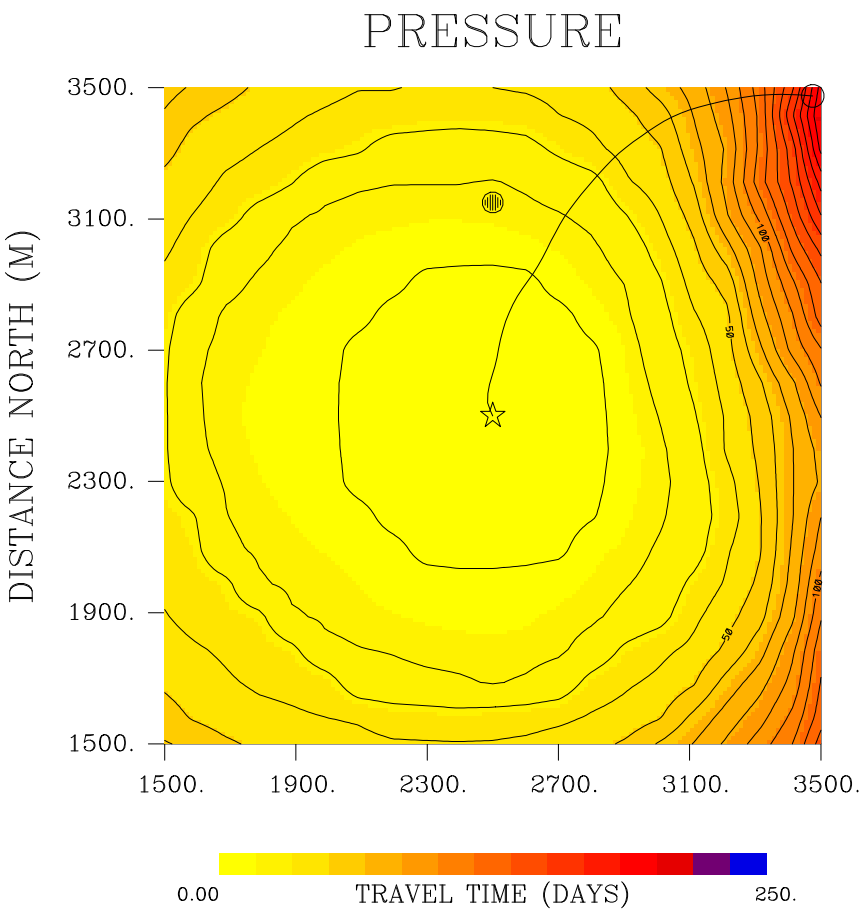
PRESSURE
DISTANCE NORTH (M)
3500.
3100.
2700.
2300.
1900.
1500.
1500.
1900.
2300.
2700.
3100.
3500.
100
50
50
100
0.00
TRAVEL TIME (DAYS)
250.

B.

Figure 18.

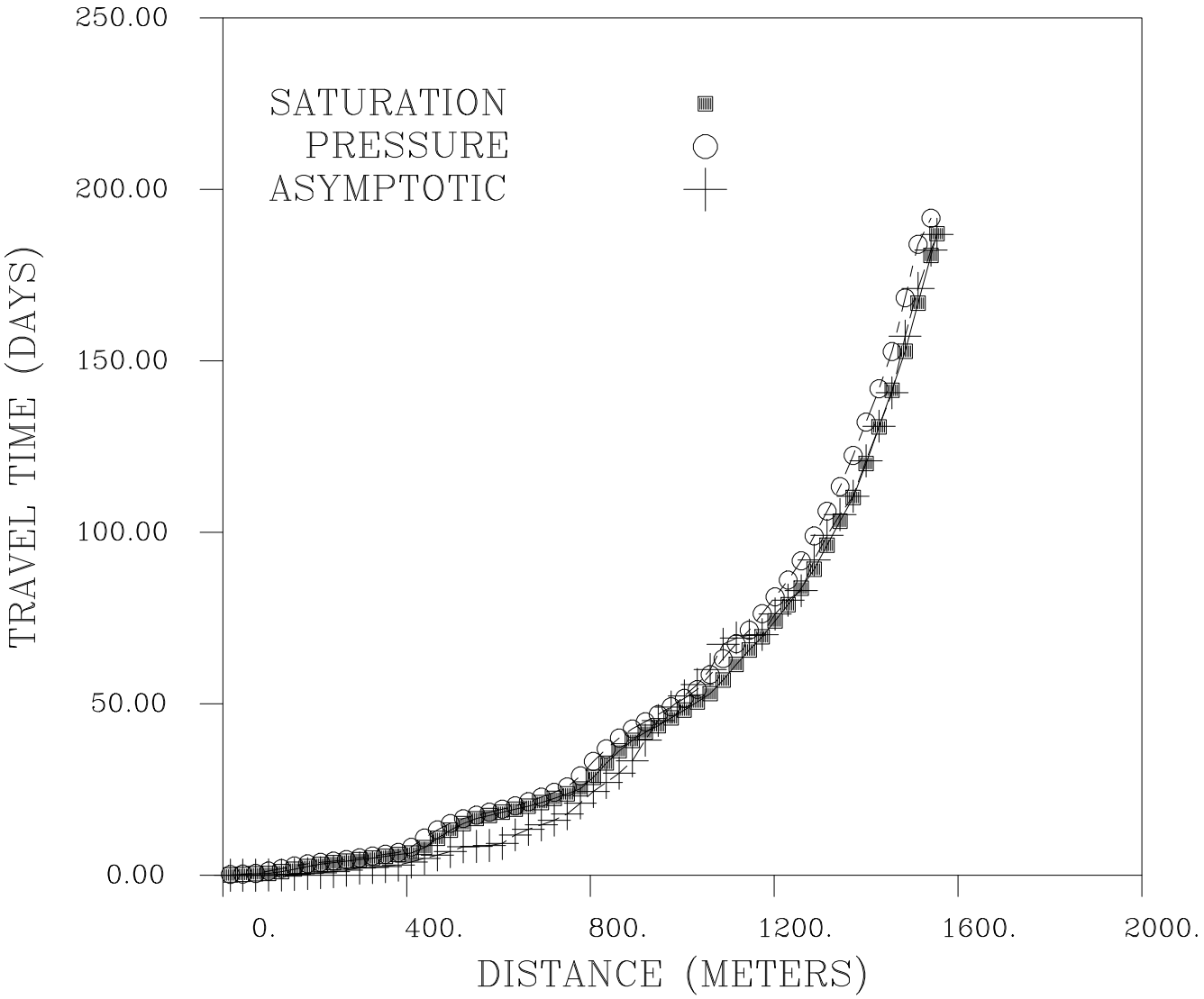
250.00
200.00
150.00
100.00
50.00
0.00
TRAVEL TIME (DAYS)
SATURATION
PRESSURE
ASYMPTOTIC
0.
400.
800.
1200.
1600.
2000.
DISTANCE (METERS)

Figure 19.

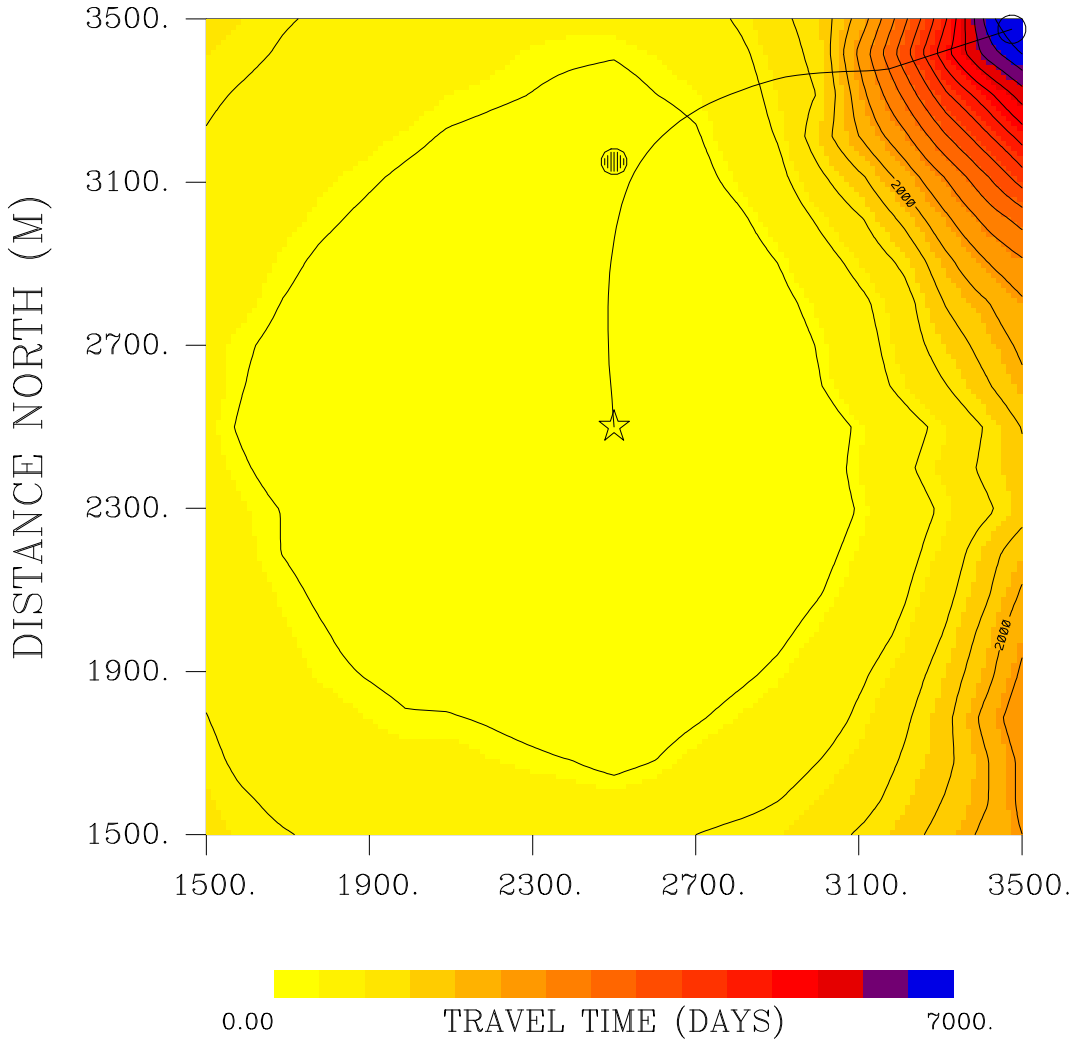
DISTANCE NORTH (M)
3500.
3100.
2700.
2300.
1900.
1500.
1500.
1900.
2300.
2700.
3100.
3500.
2000
2000
0.00
TRAVEL TIME (DAYS)
7000.

Figure 20.

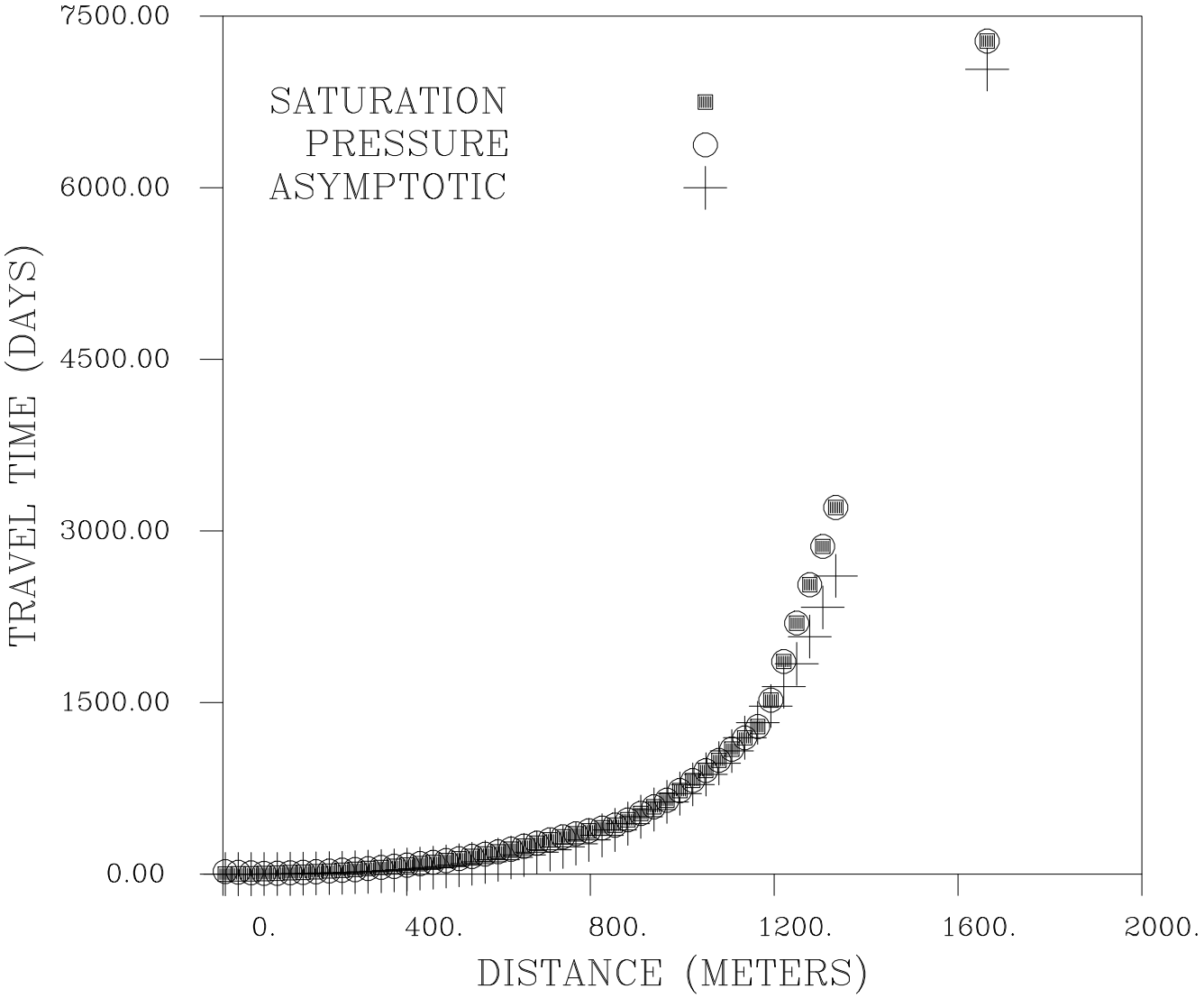
7500.00
6000.00
4500.00
3000.00
1500.00
0.00
TRAVEL TIME (DAYS)
SATURATION
PRESSURE
ASYMPTOTIC
0.
400.
800.
1200.
1600.
2000.
DISTANCE (METERS)

Figure 21.

DISCLAIMER